THERMOELECTRIC EFFICIENCY IN MODEL NANOWIRES

A THESIS

SUBMITTED TO THE DEPARTMENT OF PHYSICS

AND THE GRADUATE SCHOOL OF ENGINEERING AND SCIENCE

OF BILKENT UNIVERSITY

IN PARTIAL FULFILLMENT OF THE REQUIREMENTS

FOR THE DEGREE OF

MASTER OF SCIENCE

By

Sabuhi Badalov

August, 2013

I certify that I have read this thesis and that in my opinion it is fully adequate, in scope and in quality, as a thesis for the degree of Master of Science.

Prof. Dr. Oğuz Gülseren(Advisor)

I certify that I have read this thesis and that in my opinion it is fully adequate, in scope and in quality, as a thesis for the degree of Master of Science.

Assoc. Prof. Dr. Ceyhun Bulutay

I certify that I have read this thesis and that in my opinion it is fully adequate, in scope and in quality, as a thesis for the degree of Master of Science.

Assist. Prof. Dr. Cem Sevik

Approved for the Graduate School of Engineering and Science:

Prof. Dr. Levent Onural
Director of the Graduate School

ABSTRACT

THERMOELECTRIC EFFICIENCY IN MODEL NANOWIRES

Sabuhi Badalov
M.S. in Physics
Supervisor: Prof. Dr. Oğuz Gülseren
August, 2013

Nowadays, the use of thermoelectric semiconductor devices are limited by their low efficiencies. Therefore, there is a huge amount of research effort to get high thermoelectric efficient materials with a fair production value. To this end, one important possibility for optimizing a material's thermoelectric properties is reshaping their geometry. The main purpose of this thesis is to present a detailed analysis of thermoelectric efficiency of 2 lead systems with various geometries in terms of linear response theory, as well as 3 lead nanowire system in terms of the linear response and nonlinear response theories. The thermoelectric efficiency both in the linear response and nonlinear response regime of a model nanowire was calculated based on Landauer-Büttiker formalism. In this thesis, first of all, the electron transmission probability of the system at the hand, i.e. 2 lead or 3 lead systems are investigated by using R-matrix theory. Next, we make use of these electron transmission probability of model systems to find thermoelectric transport coefficients in 2 lead and 3 lead nanowires. Consequently, the effect of inelastic scattering is incorporated with a fictitious third lead in the 3 lead system. The efficiency at maximum power is especially useful to define the optimum working conditions of nanowire as a heat engine. Contrary to general expectation, increasing the strength of inelastic scattering is shown to be a means of making improved thermoelectric materials. A controlled coupling of the nanowire to a phonon reservoir for instance could be a way to increase the efficiency of nanowires for better heat engines.

Keywords: Thermoelectric effects, Quantum wires, Electron and Heat transport, Scattering theory, R-matrix theory, Transport properties, Nanoscale systems .

ÖZET

MODEL NANOTELLERDE TERMOELEKTRIK VERIMLILIK

Sabuhi Badalov
Fizik, Yüksek Lisans
Tez Yöneticisi: Prof. Dr. Oğuz Gülseren
Ağustos, 2013

Günümüzde, termoelektrik yarı iletken cihazların kullanımı düşük verimlilik ile sınırlıdır. Bu nedenle, son zamanlarda yüksek verimli termoelektrik malzemeleri uyğun bir maliyeti ile üretilmesi için yoğun araştırmalar sürmektedir. Yeni daha yüksek termoelektrik verimli malzemeler bulmanın yanında bir malzemenin geometrisini yeniden şekillendirerek termoelektrik özelliklerini geliştirmek üzerinde çalışılan metodlardan birisidir. Bu tezin temel amacı çeşitli geometrik yapılarda 2 bağlama telli sistemlerde lineer yanıt teorisi açısından ve 3 bağlama telli sistemlerde lineer ve lineer olmayan yanıt teorisi açısından termoelektrik verimliliğin ayrıntılı bir analizini sunmaktır. Model nanotel için lineer ve lineer olmayan yanıt rejimindeki termoelektrik verimlilik Landauer-Bütiker formulasyonu kullanılarak hesaplanmıştır. Bu tezde, ilk olarak 2 bağlı telli ve 3 bağlı telli sistemler için elektron iletim olasılığını R-matris teorisini kullanarak hesablandı. Sonra bunları kullanarak 2 bağlı telli model sistemlerinde elektron iletim olasılığından termoelektrik iletim katsayısı elde edildi. Sonraki adımda ise 3 bağlı tel sisteminde esnek olmayan saçılmanın etkisi üçüncü hayali bağın katılmasıyla incelendi. Maksimum güçte ki verimliliyi bir ısı motoru olarak nanotel en uyğun çalışma koşulları tanımlamak için özellikle yararlıdır. Genel beklentinin aksine, esnek olmayan saçılmanın gücünün artması gelişmiş termoelektrik malzemeler elde edilmesi için önemli olduğu gösterilmiştir. Örneğin bir nanoteli fonon rezervuarına kontrollü olarak etkileştirmek nanotellerin verimini artırarak daha iyi ısı motorları elde etmek için bir yol olabilir.

Anahtar sözcükler: Termoelektrik etkiler, Kuantum teller, Elektron ve Isı iletimi, Saçılma teorisi, R-matris teorisi, İletim özellikleri, Nano ölçekli sistemler .

Acknowledgement

I would never have been able to finish my dissertation without the guidance of my committee members, support from my friends and my family.

I would like to express my deepest gratitude to my supervisor, Prof. Dr. Oğuz Gülseren, who has supported me throughout this thesis with his ordinary diligence and knowledge. I attribute the level of my Masters degree to his encouragement and effort and without him this thesis, too, would not have been completed or written. One simple could not wish for a better or friendlier supervisor.

I would also like to thank Assoc. Prof. Dr. Ceyhun Bulutay and Assist. Prof. Dr. Cem Sevik for their time to read and review this thesis. Possdoc of our group Gursoy B. Akguc deserves special thanks. He has been always willing and high-minded to explain me something I struggled in my research works.

I would like to acknowledge Physics Department and all faculty members, staff graduate students especially S.Kaya, R.Bahariquşçu, N.Mehmood for their support and friendship.

Furthermore, a special thanks goes to my group mate, H.Ş.Şen, who helps me to assemble the parts and gave suggestion about programming. A special thanks also to my group members M.C.Gunendi, Y.Korkmaz, M.Erol, İ.C.Oğuz for their friendship and collaboration.

Last but not the least, I would also like to thank my father V.Badalov, my mother D.Badalova and my sister F.Badalova for the support they provided me through my entire life. I surmount all of problems and difficulties thanks to their efforts.

Contents

List of Figures

Chapter 1

Introduction

Until last three decades, global sustainable energy was thought of simplistically from the point of availability relative to the rate of use. These days, as part of the ethical framework of sustainable development, including particularly concerns about global warming, other aspects are also very significant. The world's demand for energy has become a very important in terms of causing a serious increasing political and social political unrest. It is not hard to anticipate that one of the major problems of 21^{st} century will be as fossil fuel provides decrease and world demand increases. Using efficient thermoelectric generators to reuse heat wasted from our day to day activities is one way of fulfilling our electricity demands. Figure 1.1 represents the efficiency of geothermal, industrial waste, solar, nuclear and coal heat engines in combination with some thermoelectric conversion technologies. Each of these technologies have possibility to be optimised approaching Carnot limit in the future, but it is possibility to some extent [1–3].

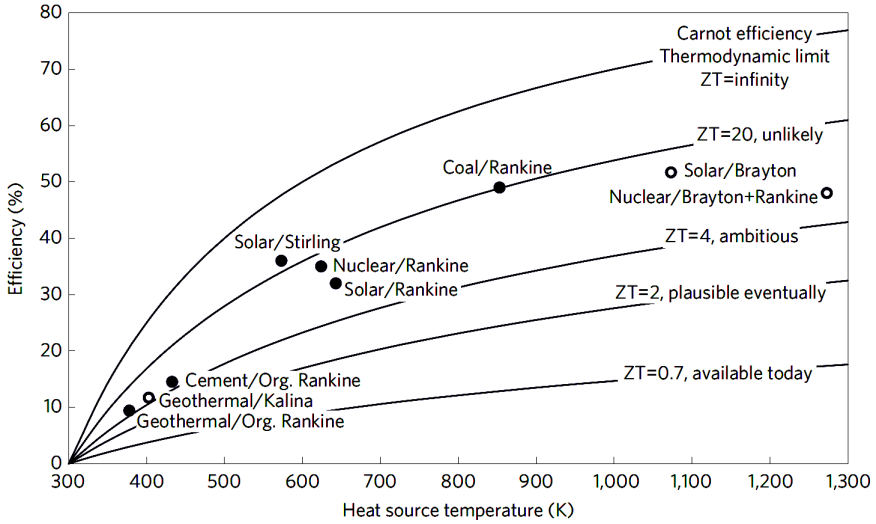

Figure 1.1: Diagram showing the power generation efficiencies of different technologies. Reproduced from reference [1].

Despite the fact that thermoelectric semiconductor devices is limited 1/3 of the maximum possible Carnot efficiency, automotive exhaust, industrial processes, and home heating all generate considerable amount of unused waste heat that could be converted to electricity by using thermoelectric materials. Heat conductivity of materials attract intense research attention as a result of its contribution to the development of modern electronics in terms of longer life, smaller size, high reliability, low maintenance requirement and noiseless electronic products. That is why, producers are willingness to utilize thermoelectric materials in automobile and home air conditioners, refrigerators, military equipment, space stations, spacecraft and so forth with regard to its advantage features. Thermoelectric phenomena provides a method for heating and cooling materials,are expected to play an increasingly important role in meeting the energy challenge of the future. Improving the efficiency of thermoelectric semiconductor devices significantly makes it to be part of the solution to high energy demand today [1–3].

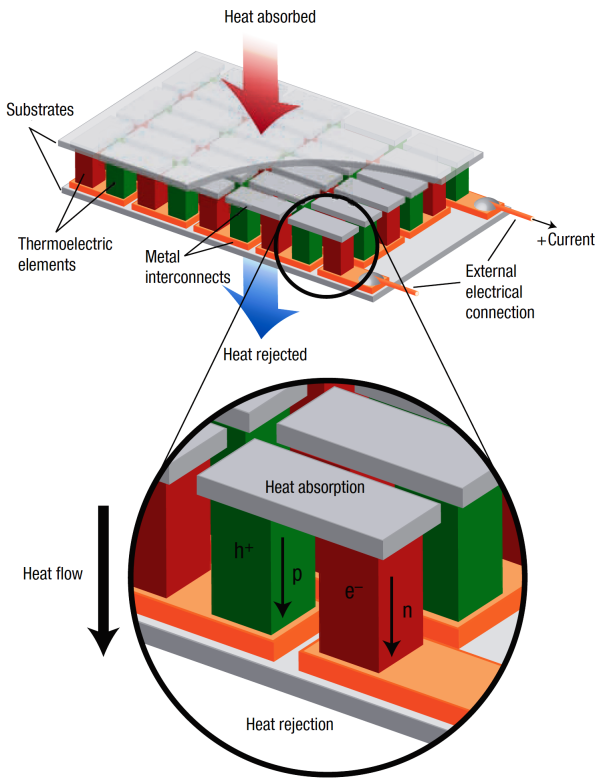

Figure 1.2: Diagram showing the operation all principles of thermoelectric components for power generation and cooling. Reproduced from reference [2].

The basic principle of energy conversion of thermoelectric semiconductor devices is shown in Fig 1.2 consists of p-type and n-type components connected with each other. When heat is supplied to it, a temperature gradient ΔT produces a voltage $V = \alpha\Delta T$ it generate power to external system so the devices become a generator. It also acts as a cooler (Peltier cooler), when an external DC current (I) supplied to it by driving heat $Q = \alpha TI$ out. This possible thermoelectric refrigerant feature is used in home and automobile air conditioners and in refrigerators [1, 2].

Generally, low dimensionality plays an increasingly irreplaceable role for the development of the next generation of thermoelectric materials [4, 5]. Silicon nanowires with rough surfaces [6, 7], multilayered carbon nanotubes/polymer thermoelectric fabrics [8], multilayered structures to adjust heat conductance [9],

and carbon nanoribbons [10] are some examples of favorable thermoelectric systems compared to bulk semiconductor materials. More complex geometries [2] and the spin degree of freedom are also a main part of research [11]. Silicon is one of the preferred candidate materials because of its established technological importance [12]. A silicon nanowire can be considered a heat engine if connected to a load, that is to say converting heat energy to work using electrons.

Long range correlation disorder plays equally important role as nanowire dimension in choosing efficient Fermi energies for heat engines made of SiO_2 nanowire [13, 14]. A perfect nanowire which does not have surface scattering would only allow extracting work at the opening of new channels, with decreasing efficiencies after the first one thanks to parasitic effects [5, 15]. This dependence may be possible owing to the strong dependence of phononic part of thermal transport on disorder [9, 16].

Specifically, we model non-coherent effects like electron-electron interaction and electron-phonon interaction for a perfect nanowire. We use a Landauer-Büttiker formalism with a fictitious third lead to incorporate the non-coherent scattering [17–19]. The multi-lead systems, specifically 3-lead systems, were recently studied for thermal rectification [20, 21], and an increase in thermoelectric efficiency which is owing to the broken symmetry was reported [22,23]. The linear response theory of 3-lead system was studied as well [24]. However, to the best of our knowledge, the nonlinear response of this system is studied in this work the first time.

To begin with, we use the reaction matrix formulation to solve the Schrödinger equation in our model 2 lead and 3 lead systems [25, 26]. Drichlet boundary condition solution instead of the standard Neuman boundary condition solution in all boundaries is used to obtain the bases [27]. Next, we utilize the transmission probability of various geometry 2 lead nanowire with linear response theory to get conductance G, thermal conductance k/L_0T, the thermopower S, and ZT. Next, we compare three type 2 lead geometry with regard to these coefficients. Later, we consider both isotropic and adiabatic processes to calculate the nonlinear power and efficiencies, and compare these with the linear response results. We do not

see much difference between these processes for the parameter space we used. We control the coupling of nanowire to a phonon reservoir by adjusting the potential barrier. The effect of the strength of inelastic scattering is discussed in this way. We find a multitude of gate voltages at which efficiency at local power max is suitable enough to run nanowire as a heat engine; and with increasing strength of inelastic scattering these positions proliferate.

The efficiency of thermoelectricity can be given in terms of the figure of merit, $ZT = GTS^2/\kappa$, where G is electrical conductivity, S is the Seebeck coefficient, also called the thermoelectric power, κ is the thermal conductance, which is the sum of the electronic contribution κ_e and the phononic contribution conductance κ_p ., and T is the absolute temperature. In the case of a heat engine, process time and drawn power can be important as well. For instance, for a reversible process, even one can get maximum possible efficiency, but this requires an infinite amount of time to produce [28, 29]. In this case, a more illustrative efficiency definition is needed to characterize it as a heat engine. That is why, we look at the efficiency at max power in 3 lead system.

Initially, we give the explanation R-matrix method with brief summary transmission probability in 1-D barrier and Landauer-Bütuker formalism in chapter 2. Then in chapter 3, we state outcome of effects of changed geometries of 2 lead system on thermoelectric efficiency of nanowire. Next, in chapter 4, we present results of effects of inelastic scattering on thermoelectric efficiency of nanowires. Finally, the thesis is concluded and discussed with summary in chapter 5.

Chapter 2

Methods and Formalism

2.1 R-matrix Method

Scattering states play a main role in electron transport, so they are essential and mobility simulations and calculations. The knowledge of scattering state solutions of the Schrödinger equation help us to surmount some problems as transmission electron microscopy images and simulation of scanning, tunneling. The Green's function-based approaches, the Lippmann-Schwinger method, mode matching techniques and the transfer matrix which are the most popular ones, have been developed to calculate scattering states. In order to compute the scattering states, we need forcible facility to represent tunneling currents, surface states, interface states, and latest, quantum transport in nanoscale devices [30–34]. In this work, we calculate the scattering states making use of R-matrix method, i.e. the reaction matrix method.

The general R-matrix theory, it was originally introduced to describe problems in electron-atom collisions by Massey and Mohr in the early 1930s and in nuclear reaction theory by Wigner and Eisenbud in 1947. It was mainly used in nuclear physics. R-matrix method has been proved for solving the Schrödinger equations of colliding charged particles, atoms and molecules with good resolution.Depending on the nature of interaction between projectile and target, this

method physically appears partition of space in the different regions. It is an extension of wave function continuity conditions to the rich complexity of systems. Surprisingly, many features of this method make it an attractive way to study electron transport and nanoscale phonon thermal transport in condensed matter devices and it is one of the most efficient method for solving scattering problems [27, 35–37].

In this thesis, we apply this method to find transmission probability in nanowire. The basic idea of the R-matrix theory is to divide the system into asymptotic and interaction regions. Firstly, we want to describe and briefly narrow down the R-matrix approach to one dimension for simplicity. Lets take the interaction region in [a,b] interval region and let $\Psi(x)$ state the solution of the Schrödinger equation in the whole space

$$\widehat{H}\Psi(x) = E\Psi(x), \quad \widehat{H} = -\frac{\hbar^2}{2m^*}\frac{d^2}{dx^2} + V(x), \;\; -\infty < x < \infty \tag{2.1}$$

here H is not Hermitian on the $[a, b]$ because

$$\begin{gathered}
\int \Psi_1(x)\widehat{H}\Psi_2(x)dx - \int \Psi_2(x)\widehat{H}\Psi_1(x)dx \\
= \int \Psi_1(x)\left(-\tfrac{\hbar^2}{2m^*}\tfrac{d^2}{dx^2} + V(x)\right)\Psi_2(x)dx - \int \Psi_2(x)\left(-\tfrac{\hbar^2}{2m^*}\tfrac{d^2}{dx^2} + V(x)\right)\Psi_1(x)dx \\
= -\tfrac{\hbar^2}{2m^*}\int \left[\Psi_2(x)\tfrac{d^2}{dx^2}\Psi_1(x) + \Psi_2(x)V(x)\Psi_1(x) - \Psi_1(x)\tfrac{d^2}{dx^2}\Psi_2(x) - \Psi_1(x)V(x)\Psi_2(x)\right]dx \\
= -\tfrac{\hbar^2}{2m^*}\int \left[\Psi_1(x)\Psi_2''(x) - \Psi_1''(x)\Psi_2(x)\right]dx \\
= -\tfrac{\hbar^2}{2m^*}\int d\left[\Psi_1(x)\Psi_2'(x) - \Psi_1'(x)\Psi_2(x)\right] \\
= -\tfrac{\hbar^2}{2m^*}\left[\Psi_1(x)\Psi_2'(x) - \Psi_1'(x)\Psi_2(x)\right]\Big|_a^b
\end{gathered} \tag{2.2}$$

In the $R-$ matrix theory, first set of an auxiliary function, $\phi_n(x)$, satisfying prescribed boundary conditions relating the wave function and its derivative at the boundary

$$\phi_n'(a) = \lambda_a\phi_n(a), \quad \phi_n'(b) = \lambda_b\phi_n(b), \tag{2.3}$$

is generated inside the $[a, b]$. The Schrödinger equation in $[a, b]$ becomes a discrete eigenvalue problem with these boundary conditions

$$-\frac{\hbar^2}{2m^*}\phi_n''(x) + V(x)\phi_n(x) = E_n\phi_n(x) \tag{2.4}$$

and the eigenfunctions form a complete set of states. By multiplying (2.1) by

$\phi_n(x)$ from the left and next, integrating along the $[a,b]$ interval gives as

$$-\frac{\hbar^2}{2m^*}\int_a^b \phi_n(x)\Psi''(x)dx + \int_a^b \phi_n(x)V(x)\Psi(x)dx = E\int_a^b \phi_n(x)\Psi(x)dx \tag{2.5}$$

Let's do the same thing now for Eq. (2.4) by multiplying $\Psi(x)$ from the left side of Eq. (2.4) and integrating in the $[a,b]$ region we obtain

$$-\frac{\hbar^2}{2m^*}\int_a^b \Psi(x)\phi_n''(x)dx + \int_a^b \Psi(x)V(x)\phi_n(x)dx = E_n\int_a^b \Psi(x)\phi_n(x)dx \tag{2.6}$$

Next, subtracting (2.6) from (2.5) side by side, we obtain

$$-\frac{\hbar^2}{2m^*}\int_a^b \left[\phi_n(x)\Psi''(x) - \Psi(x)\phi_n''(x)\right]dx = (E-E_n)\int_a^b \Psi(x)\phi_n(x)dx \tag{2.7}$$

Using integration by parts of the left hand side can simplify (2.7). Next, we obtain

$$-\frac{\hbar^2}{2m^*}\left[\phi_n(x)\Psi'(x) - \Psi(x)\phi_n'(x)\right]|_a^b = (E-E_n)\int_a^b \Psi(x)\phi_n(x)dx \tag{2.8}$$

$$\begin{aligned} -\tfrac{\hbar^2}{2m^*}\left[\phi_n(b)\Psi'(b) - \phi_n(a)\Psi'(a) - \phi_n'(b)\Psi(b) + \phi_n'(a)\Psi(a)\right] \\ = (E-E_n)\int_a^b \Psi(x)\phi_n(x)dx \end{aligned} \tag{2.9}$$

By expanding $\Psi(x)$ with regards to $\phi_n(x)$ in the [a,b] interval

$$\Psi(x) = \sum_{n=1}^{\infty} A_n\phi_n(x) \tag{2.10}$$

Here, the linear coefficient $\phi_n(x)$ in the $[a,b]$ region

$$A_n = \int_a^b \Psi(x)\phi_n(x)dx \tag{2.11}$$

Taking into account Eq.(2.9) in Eq.(2.11), we obtain

$$A_n = -\frac{\hbar^2}{2m^*}\cdot\frac{1}{E-E_n}\left[\phi_n(b)\Psi'(b) - \phi_n(a)\Psi'(a) - \phi_n'(b)\Psi(b) + \phi_n'(a)\Psi(a)\right] \tag{2.12}$$

By considering Eq.(2.12) in Eq.(2.11), the wave function in the box is like that

$$\begin{aligned} \Psi(x) = -\tfrac{\hbar^2}{2m^*}\sum_{n=1}^{\infty}\tfrac{1}{E-E_n}\left[\phi_n(b)\Psi'(b) - \phi_n(a)\Psi'(a) - \phi_n'(b)\Psi(b)\right. \\ \left. + \phi_n'(a)\Psi(a)\right]\phi_n(x) = -\tfrac{\hbar^2}{2m^*}\left(\sum_{n=1}^{\infty}\tfrac{\phi_n(b)\phi_n(x)}{E-E_n}\Psi'(b) - \sum_{n=1}^{\infty}\tfrac{\phi_n(a)\phi_n(x)}{E-E_n}\Psi'(a)\right. \\ \left. - \sum_{n=1}^{\infty}\tfrac{\phi_n'(b)\phi_n(x)}{E-E_n}\Psi(b) + \sum_{n=1}^{\infty}\tfrac{\phi_n'(b)\phi_n(x)}{E-E_n}\Psi(a)\right) \\ = R(b,x)\Psi'(b) - R(a,x)\Psi'(a) - \overline{R}(b,x)\Psi(b) + \overline{R}(a,x)\Psi(a) \end{aligned} \tag{2.13}$$

where the "$R-$matrix" is defined as

$$R(x,x') = -\frac{\hbar^2}{2m^*}\sum_{n=1}^{\infty}\frac{\phi_n(x)\phi_n(x')}{E-E_n} \tag{2.14}$$

and

$$\overline{R}(x,x') = -\frac{\hbar^2}{2m^*}\sum_{n=1}^{\infty}\frac{\phi'_n(x)\phi_n(x')}{E-E_n} \tag{2.15}$$

There are two cases (2.14) and (2.15), these depend on the boundary conditions (Neuman and Drichlet) of problem which one we can use in our problem easily [37]. It is crucial not to forget that the expansion Eq. (2.10) is valid on the $[a,b]$ closed interval but the expansion

$$\Psi'(x) = \sum_{n=1}^{\infty} A_n\phi'_n(x) \tag{2.16}$$

(provided that $\sum_{n=1}^{\infty} A_n\phi'_n(x)$ is uniformly convergent) is only valid for the (a,b) open interval because in general the boundary condition is different for Ψ and ϕ_n.

It seems that Eq.(2.5) can be solved owing to R-matrix method and we can also calculate Eq.(2.13) the wave function in the [a,b] interval region. Equation (2.12) involves the values of the wave function and the first derivative of the wave function on the boundary, but these are known from the known asymptotic wave functions.

2.1.1 Numerical calculation with the R-matrix theory in 1-D barrier

For the sake of completeness, before starting to show the results obtained in this thesis, briefly we will evoke the spirit of the method by presenting a trivial one-dimensional ($1D$) example in figure 2.1. This example's purpose is that to see how this method give us very good result in well-known exact result of this problem.

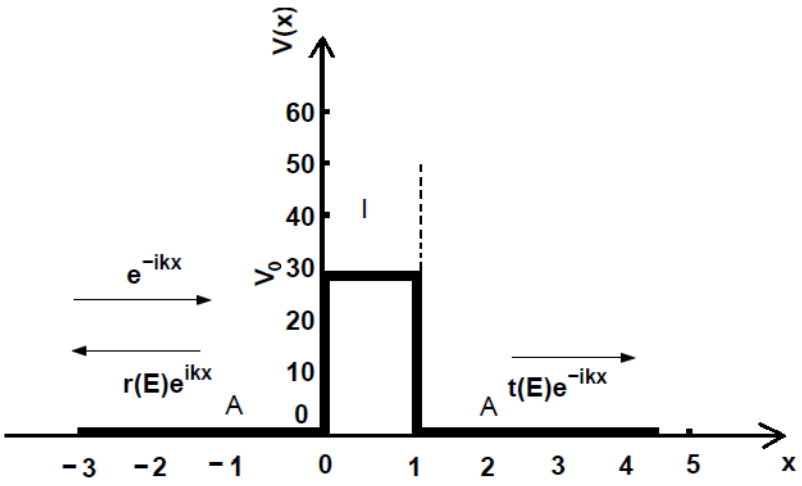

Figure 2.1: The electron scattering in 1D barrier system: A the asymptotic regions, I indicates the interaction region.

This problem is well-known problem and is calculated analytically in quantum physics. That is why, we did not want attach here analytical solution of these problem. The exact $S-$matrix can be found in this case and the transmission probability is given by

$$T_{exact}(E) = \frac{1}{1 + \frac{V_0^2 \sin^2 k'a}{E(E-V_0)}} \tag{2.17}$$

where $k' = \sqrt{\frac{2m(E-V_0)}{\hbar^2}}$ for a constant potential step of height V_0 and thickness of potential barrier a is 1. Numerically we use a basis for the reaction region (I in Fig. 1.1), which is given by $cos(n\pi x)$, $n = 0, 1, ..., \infty$. $x_l = 0$ and $x_r = 1$ have been chosen. The wave function and eigenvalue of this problem are

$$\phi_n(x) = \begin{cases} \sqrt{\frac{2}{a}} \cos \frac{n\pi x}{a} , & n = 1, 2, 3, \ldots \infty \\ \frac{1}{\sqrt{a}} , & n = 0 \end{cases} \tag{2.18}$$

and

$$E_n = \frac{\hbar^2}{2m} \cdot \frac{n^2\pi^2}{a^2} + V_0 \tag{2.19}$$

Using Neuman boundary condition and (2.17),(2.18) in (2.13), the $R-$ matrix elements are given by

$$\begin{aligned} R_{rr} &= \frac{1}{E-V_0} + \sum_{n=1}^{\infty} \frac{2}{E-n^2\pi^2-V_0} = R_{ll}, \\ R_{rl} &= \frac{1}{E-V_0} + \sum_{n=1}^{\infty} \frac{2\cos(n\pi)}{E-n^2\pi^2-V_0} = R_{lr}. \end{aligned} \tag{2.20}$$

This series should be truncated at some finite value for a numerical calculation; $j = 1000$, $V_0 = 30$ is used in Fig. 2.2. In scattering calculation, we must know asymptotic solution. For this problem at Neuman boundary condition, R-matrix is related to scattering matrix as

$$S = \begin{pmatrix} S_{ll} & S_{lr} \\ S_{rl} & S_{rr} \end{pmatrix} = U_k^{\dagger} \cdot \frac{1_M - iR_{a,b}}{1_M + iR_{a,b}} \cdot U_k^{\dagger} \tag{2.21}$$

If we consider (2.19) in (2.20), we can obtain

$$S = \begin{pmatrix} 1 & 0 \\ 0 & e^{-ik} \end{pmatrix} \frac{\begin{pmatrix} 1 & 0 \\ 0 & 1 \end{pmatrix} - ik \begin{pmatrix} R_{rr} & R_{rl} \\ R_{lr} & R_{ll} \end{pmatrix}}{\begin{pmatrix} 1 & 0 \\ 0 & 1 \end{pmatrix} + ik \begin{pmatrix} R_{rr} & R_{rl} \\ R_{lr} & R_{ll} \end{pmatrix}} \begin{pmatrix} 1 & 0 \\ 0 & e^{-ik} \end{pmatrix} \tag{2.22}$$

and the transmission probability is

$$T = |(S_{r,l})|^2 \tag{2.23}$$

We plot both of result T_{exact} and $|(S_{r,l})|^2$, and we can see superiority of this method with compare exact solution in Fig 2.2.

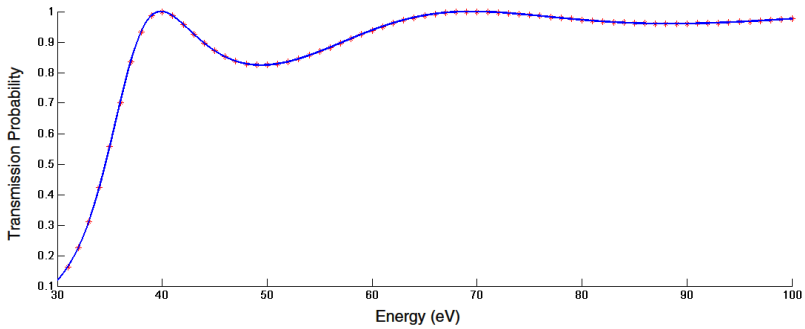

Figure 2.2: The exact result shows Transmission probability as a function of energy, and red stars denotes the numerical calculation.

2.2 Landaur-Buttiker formalism of thermoelectricity

The Landauer-Büttiker method establishes the fundamental relation between the wave functions of noninteracting quantum system and its conducting properties. For brief information, the nonlinear and linear response theory is mentioned via Landauer-Büttiker approach [13, 15]. Figure of merit ZT is related to the thermoelectric accessible efficiency. The following relation the maximum efficiency η with ZT is defined as

$$\eta = \eta_C \cdot \frac{\sqrt{1+ZT}-1}{\sqrt{1+ZT}+\frac{T_c}{T_h}} \tag{2.24}$$

where $\eta_c = 1 - \frac{T_c}{T_h}$ is thermodynamical maximal Carnot efficiency [5, 38]. We can understand the sources of irreversible conversion losses owing to the development of strategies to realize operation near η_c. However, efficiency near η_c requires near-reversible operation, a limit where the output absolutely to zero, hence it does not practical value. To understand the relationship between efficiency and power production it causes intense interest in practical applications. In this context, the regarding fundamental efficiency limit is that

$$\eta_{CA} = \sqrt{1-\frac{T_c}{T_h}} \tag{2.25}$$

which is known the Curzon-Ahlborn limit [5]. The thermoelectric efficiency is also defined as

$$\eta = \frac{P_{out}}{\dot{q}_h} \tag{2.26}$$

where P_{out} is maximum power output.

$$P_{max} = I\Delta V \tag{2.27}$$

The maximum heat current is defined as

$$\dot{q}_{max} = (\dot{q}_h - \dot{q}_c) \tag{2.28}$$

So a more illustrative efficiency definition is needed to characterize it as a heat engine. Thus, looking at the efficiency at maximum plays a important role in

thermoelectricity. However, archiving this calculation we must use nonlinear Landauer thermodynamic approach for one propagating mode shown below

$$I = \frac{2e}{h} \int t(E)(f_h - f_c)dE, \tag{2.29}$$

$$\dot{q}_h = \frac{2}{h} \int t(E)(E - \mu_h)(f_h - f_c)dE, \tag{2.30}$$

$$\dot{q}_c = \frac{2}{h} \int t(E)(E - \mu_c)(f_h - f_c)dE, \tag{2.31}$$

where $\dot{q}_h$ and $\dot{q}_c$ are the the heat flow and cold flow from hot and cold reservoirs, respectively, h is the Planck constant, $t(E)$ is the transmission. The equilibrium Fermi-Dirac distributions for the contacts f_h and f_c are defined as

$$f_{h/c} = \Big[\exp((E - \mu_{h/c})/k_B T_{h/c}) + 1\Big]^{-1}, \tag{2.32}$$

where $\mu_{h/c} = \mu + V_\alpha$ is the chemical potential of heat and cold side, respectively, and V_α is the bias on each side [13].

Let us presume that only two reservoirs are present. When the temperature difference and the bias are very to each other, it is possible to expand Fermi energy in Taylor series and approximate both the current and the heat extraction rate with regard to one bias and temperature parameter. In equilibrium, the reservoirs are at chemical potential E_F and temperature T. In the linear response regime, the current I and heat flow q in the following equation

$$\begin{aligned} I &= G\Delta\mu/e + L\Delta T, \\ \dot{q} &= -M\Delta\mu/e - K\Delta T, \end{aligned} \tag{2.33}$$

where ΔT is the temperature difference between the contacts, $\Delta\mu$ is the chemical potential difference, G is the electric conductance, and T is the temperature. M and L are related by an Onsager relation, in which there is not magnetic field

$$M = -LT, \tag{2.34}$$

Eq.(2.33) is often re-expressed with the current I rather than the electrochemical potential $\Delta\mu$ by the following equation

$$\begin{aligned} \Delta\mu/e &= RI + S\Delta T, \\ \dot{q} &= -\Pi I + k\Delta T, \end{aligned} \tag{2.35}$$

The resistance R is the reciprocal of the isothermal conductance G. The thermopower S is defined as

$$S \equiv \left(\frac{\triangle\mu/e}{\triangle T}\right)_{I=0} = -\frac{L}{G}, \tag{2.36}$$

The Peltier coefficient Π, defined as

$$\Pi \equiv \left(\frac{\dot{q}}{I}\right)_{I=0} = -\frac{M}{G} = ST, \tag{2.37}$$

is a proportional to the thermopower S in view the Onsager relation (2.34). The electronic contribution to the thermal conductivity κ is defined as

$$k \equiv -\left(\frac{\dot{q}}{\triangle T}\right)_{I=0} = -K\left(1 + \frac{S^2GT}{K}\right) \tag{2.38}$$

The thermoelectric coefficients are given in the Landauer-Büttiker formalism by

$$G = -\frac{2e^2}{h}\int_0^\infty dE \frac{\partial f}{\partial E} t(E), \tag{2.39}$$

$$L = -\frac{2e^2}{h}\frac{k_B}{e}\int_0^\infty dE \frac{\partial f}{\partial E} t(E)(E - E_F)/k_BT, \tag{2.40}$$

$$\frac{K}{T} = \frac{2e^2}{h}\left(\frac{k_B}{e}\right)^2 \int_0^\infty dE \frac{\partial f}{\partial E} t(E)\left[(E - E_F)/k_BT\right]^2, \tag{2.41}$$

where f is a Fermi function defined as

$$f = \left[\exp((E - E_F)/k_BT) + 1\right]^{-1}, \tag{2.42}$$

These integrals are convolution of t(E) which is a transmission probability of a quantum point contact modelled as an ideal electron waveguide with step function energy dependence

$$t(E) = \sum_{n=1}^{\infty} \theta(E - E_n), \tag{2.43}$$

The energies E_n are given by

$$E_n = V_0 + \left(n - \frac{1}{2}\right)\hbar\omega_y, \tag{2.44}$$

To characterize a thermoelectric material, ZT figure of merit is used commonly, its expression is as

$$ZT = GS^2T/k, \tag{2.45}$$

Taking into account all of factors about linear Landauer-Büttiker approach, we can obtain a result shown in Fig 2.3.

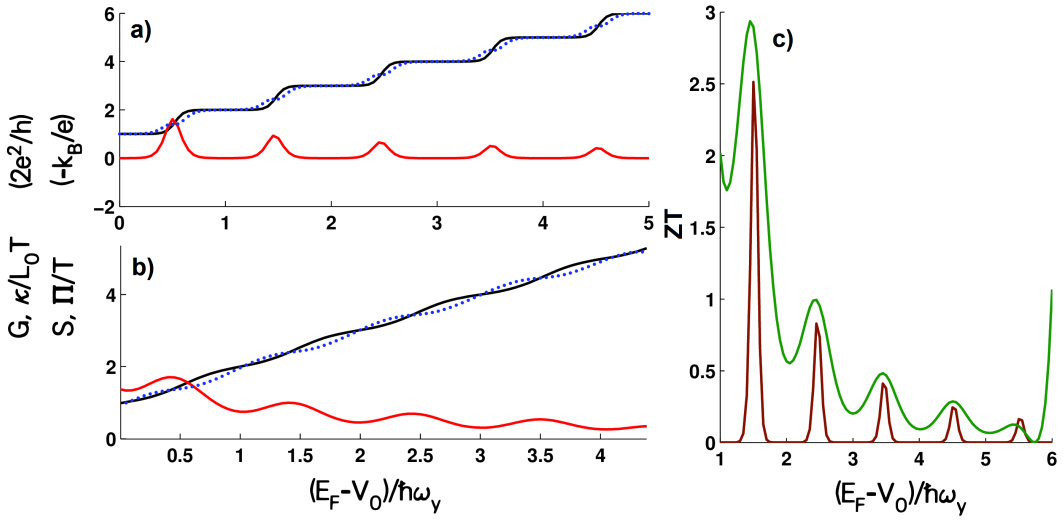

Figure 2.3: Electrical conductivity G(black curve), thermal conductance k/L_0T where L_0T is Lorentz number (broken blue curve), and the thermopower S and Peltier coefficient Π (red curve) for a quantum point contact with step function $t(E)$ as Fermi function at (a) 1K and (b) 4K. The parameter used in the calculation is $\hbar\omega_y = 2meV$. The figure of merit ZT (brown curve at (c) 1K, green curve at (c) 4K

Chapter 3

Thermoelectric Efficiency in 2-lead system

3.1 Model System

In chapter 2, we gave the derivation of expressions of R-matrix method and a simple example, in order to illustrate the theoretical framework with applications which can be easily reproduced by the reader. In this section, we present more ambitious applications of the R-matrix theory in condensed matter physics. The basic foundation R-matrix theory lies on the expansion of the reaction regime wavefunction onto a complete and discrete set of basis. This set satisfies arbitrary boundary coordination at the interfaces between the asymptotic regions and reaction region. In principle the R-matrix approach does not depend on choose of boundary conditions at the interface between reaction and asymptotic regions. However, based on traditional R-matrix we choose Neuman boundary condition for choice of basis sets in the interface. In electron waveguides utilizing the Dirichlet boundary conditions results more convergent solution, because reaction regions have complicated distributions of potential and coupling to external leads.

Our model systems shown in Fig.2.1 consist of stub, straight or ideal, and

concave nanowires. In this model, two straight leads called the left (l) and right (r) asymptotic regions are connected with a rectangular cavity called the reaction region. We can describe projection operators

$$\begin{aligned}
\widehat{Q} &= \int_{\frac{-W_2}{2}}^{\frac{W_2}{2}} dx \int_{-\infty}^{\infty} dy \mid x,y >< x,y \mid, \\
\widehat{P}_l &= \int_{-\infty}^{\frac{-W_2}{2}} dx \int_{-\infty}^{\infty} dy \mid x,y >< x,y \mid, \\
\widehat{P}_r &= \int_{\frac{W_2}{2}}^{\infty} dx \int_{-\infty}^{\infty} dy \mid x,y >< x,y \mid
\end{aligned} \tag{3.1}$$

The operator $\widehat{Q}$ projects into the reaction region where as $\widehat{P}_l$ and $\widehat{P}_r$ projects into the left and right asymptotic regions, respectively. These operators satisfy the conditions $\widehat{P}_l + \widehat{P}_r + \widehat{Q} = \widehat{1}, \widehat{P}_\alpha^2 = \widehat{P}_\alpha, \widehat{Q}^2 = \widehat{Q}$ and $\widehat{P}_\alpha \widehat{Q} = \widehat{Q}\widehat{P}_\alpha$ $(\alpha = l, r)$ the Hamiltonian can be described as

$$\widehat{H} = \widehat{H}_{\widehat{Q}\widehat{Q}} + \sum_{\alpha=l,r} \left(\widehat{H}_{\widehat{P}_\alpha \widehat{P}_\alpha} + \widehat{H}_{\widehat{P}_\alpha \widehat{Q}} + \widehat{H}_{\widehat{Q}\widehat{P}_\alpha} \right), \tag{3.2}$$

where generally $\widehat{H}_{\widehat{x}\widehat{x}} = \widehat{x}\widehat{H}\widehat{x}$, and the block operators $\widehat{H}_{\widehat{P}_\alpha \widehat{Q}}$ and $\widehat{H}_{\widehat{Q}\widehat{P}_\alpha}$ in Neuman boundary conditions couple the reaction and asymptotic regions. Into use Dirichlet boundary condition, we need to modify these coupling operators from the usual block form as follows

$$\widehat{H}_{\widehat{P}_\alpha \widehat{Q}} = \pm \frac{2\hbar^2}{m^*} \widehat{P}_\alpha \delta(x - x_\alpha) \widehat{\partial}_x^{\rightarrow} \widehat{Q}, \ \widehat{H}_{\widehat{Q}\widehat{P}_\alpha} = \pm \frac{2\hbar^2}{m^*} \widehat{Q} \delta(x - x_\alpha) \widehat{\partial}_x^{\leftarrow} \widehat{P}_\alpha \tag{3.3}$$

where m^* , $\widehat{\partial}_x^{\rightarrow}$ $\left(\widehat{\partial}_x^{\leftarrow}\right)$ and x_α represent effective mass of an electron, differential operators actin to the right (left) of the reaction region and the x-position of the interface between the reaction and asymptotic region respectively, and the sign $\pm$ is for $\alpha = r(l)$.

By using the projection operators, the Schrödinger equation in the reaction region takes the form

$$\left(E - \widehat{H}_{QQ}\right) \widehat{Q}|\Psi\rangle = \widehat{H}_{QP_l} \widehat{P}_l |\Psi\rangle + \widehat{H}_{QP_r} \widehat{P}_r |\Psi\rangle \tag{3.4}$$

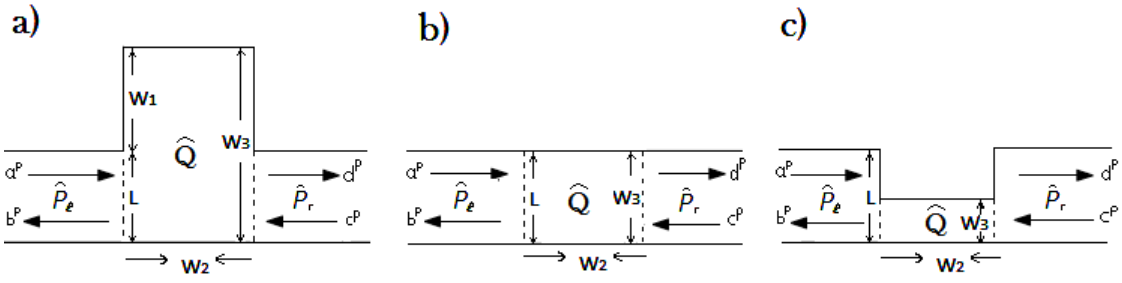

Figure 3.1: a) Stub nanowire, b) Ideal nanowire, c) Concave nanowire

and in the asymptotic regions it can be defined as

$$\begin{aligned}\left(E-\widehat{H}_{P_lP_l}\right)\widehat{P}_l|\Psi\rangle &= \widehat{H}_{P_lQ}\widehat{Q}|\Psi\rangle,\\ \left(E-\widehat{H}_{P_rP_r}\right)\widehat{P}_r|\Psi\rangle &= \widehat{H}_{P_rQ}\widehat{Q}|\Psi\rangle\end{aligned} \tag{3.5}$$

Direchlet boundary conditions are considered in the reaction region including all boundaries between the asymptotic and the reaction regions. The eigenfunction in the reaction regions are sine waves for both the $x-$ and $y-$ directions. A set of complete orthogonal basis $|\psi_{p,q}\rangle$ can be represented, which satisfy

$$\widehat{H}_{QQ}|\psi_{p,q}\rangle = E_{p,q}|\psi_{p,q}\rangle \tag{3.6}$$

in which

$$E_{p,q} = \frac{\hbar^2}{2m^*}\left(\left(\frac{p\pi}{W_2}\right)^2+\left(\frac{q\pi}{W_2}\right)^2\right) \tag{3.7}$$

$$\langle x,y|\psi_{p,q}\rangle = \begin{cases} \sqrt{\frac{2}{W_2}}\sin\left(\frac{p\pi x}{W_2}\right)\sqrt{\frac{2}{W_3}}\sin\left(\frac{q\pi y}{W_3}\right) & for \quad x_l\le x\le x_r, \quad 0\le y\le W_3 \\ 0 & for \quad otherwise \end{cases} \tag{3.8}$$

We can expand the electron scattering wavefunction $|\Psi\rangle$ with regards to the basis functions $|\psi_{p,q}\rangle$ in the reaction region for a given electron incident energy E,

$$\langle x,y|\widehat{Q}\Psi\rangle = \sum_{p=1}^{\infty}\sum_{q=1}^{\infty}\gamma_{p,q}\langle x,y|\psi_{p,q}\rangle \tag{3.9}$$

where $\gamma_{p,q}$ is an expansion coefficient. We obtain below equation with regard to using equations (3.4) and (3.9),

$$\begin{array}{c}\gamma_{p,q} = -\frac{2\hbar^2}{2m^*}\frac{1}{E-E_{p,q}}\Big[\int\int dxdy\left\{\langle\psi_{p,q}|x,y\rangle\widehat{\partial}_x^{\leftarrow}\delta(x-x_l)\langle x,y|\widehat{P}_l|\Psi\rangle\right\} \\ -\int\int dxdy\left\{\langle\psi_{p,q}|x,y\rangle\widehat{\partial}_x^{\leftarrow}\delta(x-x_r)\langle x,y|\widehat{P}_r|\Psi\rangle\right\}\Big],\end{array} \tag{3.10}$$

The wave function along the transversal direction is discredited by virtue of the hard wall boundary conditions for the upper and bottom walls of the leads on the asymptotic region:

$$\langle x,y|\widehat{P}_\alpha|\Psi\rangle = \begin{cases} \sum_{n=1}^{\infty}\chi_n^\alpha(x)\sqrt{\frac{2}{L}}\sin\left(\frac{n\pi y}{L}\right) & for \quad 0\le y\le L, \\ 0 & for \quad otherwise \end{cases} \tag{3.11}$$

where $(\alpha = l, r)$

Considering both propagating and evanescent modes for the incident energy E, the longitudinal wavefunction for the n^{th} propagating mode given by

$$\begin{array}{c}\chi_n^l(x) = \frac{a_n^p}{\sqrt{k_n}}\exp(ik_nx) - \frac{b_n^p}{\sqrt{k_n}}\exp(-ik_nx) \\ \chi_n^r(x) = \frac{d_n^p}{\sqrt{k_n}}\exp(ik_nx) - \frac{c_n^p}{\sqrt{k_n}}\exp(-ik_nx),\end{array} \tag{3.12}$$

where $k_n = \sqrt{\frac{2m^*E}{\hbar^2} - \left(\frac{n\pi}{L}\right)^2}$, a_n^p and c_n^p (b_n^p and d_n^p) are the amplitudes of incoming (outgoing) propagating modes in the leads. For the n^{th} evanescent mode, the longitudinal wave functions are

$$\begin{array}{c}\chi_n^l(x) = \frac{b_n^p}{\sqrt{\kappa_n}}\exp(\kappa_nx) \\ \chi_n^r(x) = -\frac{d_n^l}{\sqrt{\kappa_n}}\exp(-\kappa_nx),\end{array} \tag{3.13}$$

where $\kappa_n = \sqrt{\left(\frac{n\pi}{L}\right)^2 - \frac{2m^*E}{\hbar^2}}$.

When we work with Dirichlet boundary conditions, we impose continuity on the slope of the electron scattering wave function at the interfaces. This provides the condition

$$\frac{\partial}{\partial x}\chi_n^\alpha(x)|_{x=x_\alpha} = -\sum_{n'=1}^{\infty}R_{\alpha l}(n,n')\chi_{n'}^l(x_l) + \sum_{n'=1}^{\infty}R_{\alpha r}(n,n')\chi_{n'}^l(x_r), \tag{3.14}$$

where

$$R_{\alpha,\beta}(n,n') = \frac{\hbar^2}{2m^*}\sum_{p,q}\frac{u'_{p,q,n}(x)u'_{p,q,n'}(x')}{E-E_{p,q}}, \tag{3.15}$$

$$
\begin{aligned}
u_{p,q,n}(x_\alpha) &= \sqrt{\tfrac{2}{L}} \int_0^L \sin\left(\tfrac{n\pi y}{L}\right) \psi_{p,q}(x_\alpha, y) dy \\
&= \sqrt{\tfrac{2}{L}} \int_0^L \sin\left(\tfrac{n\pi y}{L}\right) \sqrt{\tfrac{2}{W_2}} \sin\left(\tfrac{p\pi x_\alpha}{W_2}\right) \sqrt{\tfrac{2}{W_3}} \sin\left(\tfrac{q\pi y}{W_3}\right) dy \\
&= \sqrt{\tfrac{2}{W_2}} \sin\left(\tfrac{n\pi x_\alpha}{W_2}\right) \tfrac{2}{\sqrt{LW_3}} \int_0^L \sin\left(\tfrac{n\pi y}{L}\right) \sin\left(\tfrac{q\pi y}{W_3}\right) dy \\
&= \sqrt{\tfrac{2}{W_2}} \sin\left(\tfrac{n\pi x_\alpha}{W_2}\right) f_{n,q},
\end{aligned}
\tag{3.16}
$$

$$
f_{n,q} = \frac{2}{\sqrt{LW_3}} \int_0^L \sin\left(\frac{n\pi y}{L}\right) \sin\left(\frac{q\pi y}{W_3}\right) dy, \tag{3.17}
$$

and

$$
u'_{p,q,n'}(x_\alpha) = \left.\frac{du_{p,q,n}(x)}{dx}\right|_{x=x_\alpha}. \tag{3.18}
$$

The summation in equation (3.15) does not uniformly converge because the numerator and the denominator are p dependence functions. Term-by-term differentiation can cause the series to diverge in equation (3.15). That is why, we take differentiation after summation is performed:

$$
R_{\alpha,\beta}(n,n') = \frac{\hbar^2}{2m^*} \left[\frac{\partial}{\partial x} \frac{\partial}{\partial x'} \left(\sum_{p,q} \frac{u_{p,q,n}(x) u_{p,q,n'}(x')}{E - E_{p,q}} \right) \right] \Bigg|_{x=x_\alpha, x'=x_\beta} \tag{3.19}
$$

Fortunately, the series in equation (3.19) is analytically separated for indexes p and q because the system is separable. Before we compute the differentiation, it permits us to take the summation over index p.

$$
\sum_{k=1}^{\infty} \frac{coskx}{k^2 - \alpha^2} = \frac{1}{2\alpha^2} - \frac{\pi}{2} \frac{\cos\alpha[(2m+1)\pi - x]}{\alpha \sin\alpha\pi}, \quad 2m\pi \le x \le (2m+2)\pi, \tag{3.20}
$$

where α is not an integer

$$
\sum_{k=1}^{\infty} \frac{coskx}{k^2 + \alpha^2} = \frac{\pi}{2} \frac{\cosh\alpha(\pi - x)}{\alpha \sinh\alpha\pi} - \frac{1}{2\alpha^2}, \quad 0 \le x \le 2\pi \tag{3.21}
$$

We compute the summation over p and obtain R-matrix elements including a summation only over the q-index thanks to the trigonometric series equation (3.20), (3.21) [39], and obtain all of R-matrix elements as

$$
\begin{aligned}
R_{ll}(n,n') = R_{rr}(n,n') &= \sum_{q=1}^{\infty} f_{q,n} f_{q,n'} k_q csc(k_q W_2) cos(k_q W_2), \\
R_{lr}(n,n') = R_{rl}(n,n') &= \sum_{q=1}^{\infty} f_{q,n} f_{q,n'} k_q csc(k_q W_2),
\end{aligned}
\tag{3.22}
$$

where $0 \leq x_\alpha, x_\beta \leq 2\pi$ and $k_q = \sqrt{\frac{2m^*E}{\hbar^2} - \left(\frac{q\pi}{W_3}\right)^2}$. Note that equation (3.19) holds when $\frac{2m^*E}{\hbar^2} > \left(\frac{q\pi}{W_3}\right)^2$. When $\frac{2m^*E}{\hbar^2} < \left(\frac{q\pi}{W_3}\right)^2$, then $k_q \to i\widetilde{k}_q$, $\widetilde{k}_q = \sqrt{\left(\frac{q\pi}{W_3}\right)^2 - \frac{2m^*E}{\hbar^2}}$, $\sin k_q x \to i \sinh \widetilde{k}_q x$ and $\cos k_q x \to \cosh \widetilde{k}_q x$.

$$\begin{aligned} R_{ll}(n,n') = R_{rr}(n,n') &= \sum_{q=1}^{\infty} f_{q,n} f_{q,n'} \widetilde{k}_q csch(\widetilde{k}_q W_2) cosh(\widetilde{k}_q W_2), \\ R_{lr}(n,n') = R_{rl}(n,n') &= \sum_{q=1}^{\infty} f_{q,n} f_{q,n'} \widetilde{k}_q csch(\widetilde{k}_q W_2) \end{aligned} \tag{3.23}$$

S-matrix for the models shown in Fig.3.1 can be calculated. The relation between the wavefunction in the two asymptotic region of nanowires is obtained from Equation (3.13). This S-matrix relates the incoming propagation modes (a_n^p and c_n^p) to the outgoing propagation modes (b_n^p and d_n^p). Using equation(3.12-3.14), equation (3.14) can be described in the following matrix form:

$$\begin{pmatrix} i(\mathbf{A}+\mathbf{B}) \\ \mathbf{D} \end{pmatrix} = -\mathbf{K}\cdot\mathbf{R}\cdot\mathbf{K}\cdot\begin{pmatrix} \mathbf{A}-\mathbf{B} \\ \mathbf{D} \end{pmatrix} \tag{3.24}$$

where the sub-column matrices [27] $\mathbf{A}, \mathbf{B}$ and $\mathbf{D}$ are as

$$\mathbf{A} = \begin{pmatrix} a_n^p \exp(ik_n x_l) \\ c_n^p \exp(-ik_n x_r) \end{pmatrix}, \qquad \mathbf{B} = \begin{pmatrix} b_n^p \exp(-ik_n x_l) \\ d_n^p \exp(ik_n x_r) \end{pmatrix} \tag{3.25}$$

and

$$\mathbf{D} = \begin{pmatrix} b_n^e \exp(\kappa_n x_l) \\ d_n^e \exp(-\kappa_n x_r) \end{pmatrix} \tag{3.26}$$

where the super-indices p and e represent the propagating and evanescent modes [27], respectively. The matrix $\mathbf{K}$ is a diagonal matrix whose elements are

$$\mathbf{K}_{n,n} = \begin{cases} \frac{1}{\sqrt{k_n}} = (\mathbf{K}_p)_{n,n} & for \quad n \leq N_p, \\ \frac{1}{\sqrt{\kappa_n}} = (\mathbf{K}_e)_{n,n} & for \quad otherwise \end{cases} \tag{3.27}$$

The R-matrix, $\mathbf{R}$, is given by

$$\mathbf{R} = \begin{pmatrix} \mathbf{R}_{PP} & \mathbf{R}_{PE} \\ \mathbf{R}_{EP} & \mathbf{R}_{EE} \end{pmatrix} \tag{3.28}$$

Let us assume that there are N_P propagating modes in the leads for a given incident energy E. The sub-matrix $\mathbf{R}_{PP}$ is given by

$$\mathbf{R} = \begin{pmatrix} R_{ll}(p,p) & R_{lr}(p,p) \\ R_{rl}(p,p) & R_{rr}(p,p) \end{pmatrix} \tag{3.29}$$

where (p,p) represents the propagating modes and it is a $2N_P \times 2N_P$ matrix. Let us assume that N_e evanescent modes are needed to obtain accurate expressions for the S-matrix. Next, $\mathbf{R}_{PE}$ is an $N_p \times N_e$ matrix, $\mathbf{R}_{EP}$ is an $N_e \times N_p$ matrix and $\mathbf{R}_{EE}$ is an $N_e \times N_e$ matrix [27].

The S-matrix connects the incoming amplitudes $\mathbf{A}$ to the outgoing amplitudes. If we solve (3.24) for $\mathbf{B}$ as a function of $\mathbf{A}$, we can write it as $\mathbf{B} = \mathbf{S} \cdot \mathbf{A}$ where the S-matrix, $\mathbf{S}$, is given by

$$\mathbf{S} = \begin{pmatrix} \mathbf{S}_{l,l} & \mathbf{S}_{l,r} \\ \mathbf{S}_{r,l} & \mathbf{S}_{r,r} \end{pmatrix} = -\frac{\mathbf{1} - i\mathbf{Z}}{\mathbf{1} + i\mathbf{Z}} \tag{3.30}$$

and $\mathbf{A}$ where the S-matrix, $\mathbf{S}$, is given by

$$\mathbf{Z} = \mathbf{K_p R_{PP} K_p} - \mathbf{K_p R_{PE} K_e} \cdot \frac{\mathbf{1}}{\mathbf{1} + \mathbf{K_e R_{EE} K_e}} \cdot \mathbf{K_e R_{EP} K_p} \tag{3.31}$$

In (3.30) and (3.31) [40], the evanescent modes are explicitly folded into the expression for the S-matrix.

We now obtain expressions for the transmission probability in the stub, ideal, and cavity nanowire system. We consider a stub nanowire with $L = 10nm, W_3 = 20nm$ and $W_2 = 20nm$, a ideal nanowire with $L = 10nm, W_3 = 10nm$ and $W_2 = 20nm$, and cavity nanowire with $L = 10nm, W_3 = 3nm$ and $W_2 = 20nm$. We use the effective electron mass $m^* = 0.05m_e$. From the S-matrix derived above, we compute the total electron transmission probability through the stub, ideal, and cavity nanowire system. The total transmission probability is obtained by

$$T = \sum_{m=1}^{N_P} \sum_{n=1}^{N_P} |(S_{r,l})_{nm}|^2 \tag{3.32}$$

The n^{th} propagating mode opens at $E_n = \frac{\hbar^2}{2m^*} \left(\frac{n\pi}{L}\right)^2$, since the wave function along the transversal direction in the leads is quantized. In order to obtain convergent results, we have included $N_e = 8$ evanescent modes.

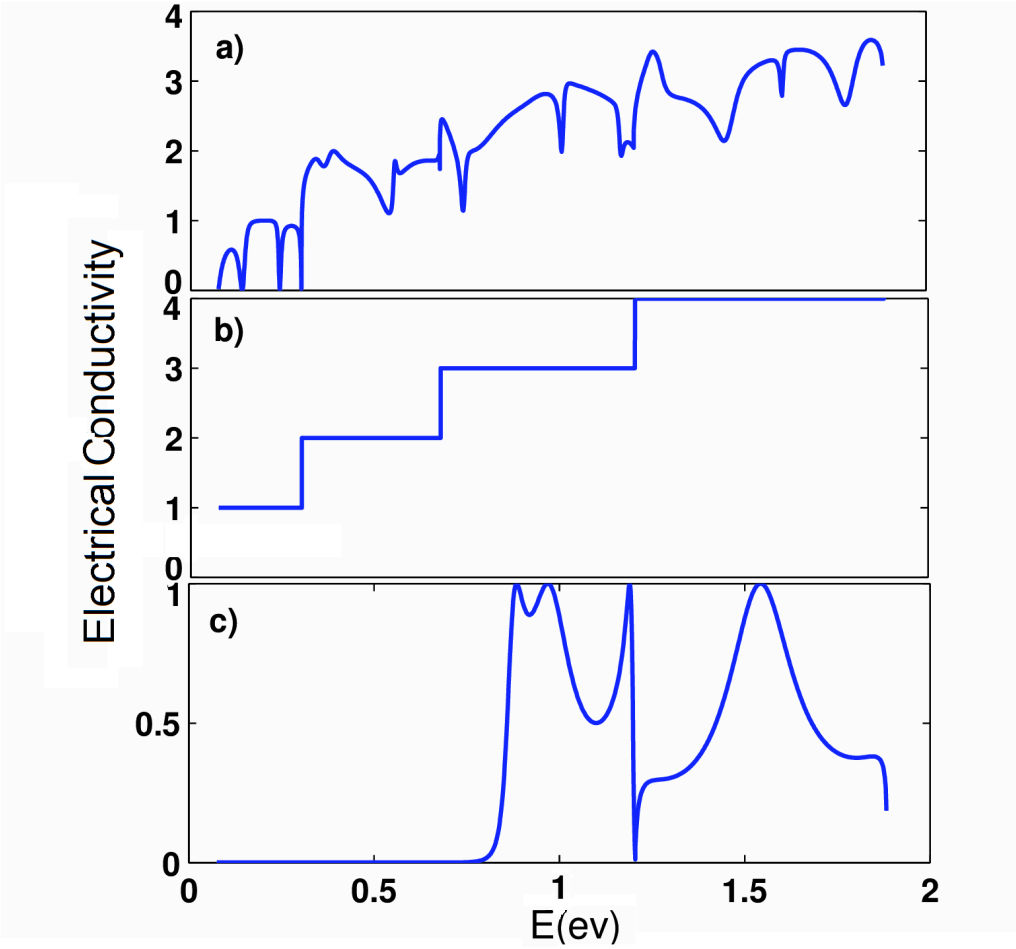

Figure 3.2: Electrical conductivity in (a) stub nanowire, (b) ideal nanowire, (c) cavity nanowire

The second propagating mode opens at $E = 0.301eV$. The third propagating mode opens at $E = 0.678eV$. The fourth propagating mode opens at $E = 1.205eV$. We can see transmission probability in stub, ideal, and cavity nanowire system in figure 3.2. For example, in figure 3.2 c), the reason of not opening of the first and second propagating modes is a narrow reaction region of cavity nanowire.

3.2 Thermoelectric Efficiency

We use the Landauer-Buttiker approach to calculate the electron transport coefficient for this system. In the linear response regime, the current I and heat flow q are related to the chemical potential difference $\triangle\mu$ and the temperature difference $\triangle T$ by the constitutive equations

$$\begin{pmatrix} I \\ \dot{q} \end{pmatrix} = \begin{pmatrix} G & L \\ LT & K \end{pmatrix} \begin{pmatrix} \triangle\mu/e \\ \triangle T \end{pmatrix} \tag{3.33}$$

The thermopower S is defined as

$$S \equiv \left(\frac{\triangle\mu/e}{\triangle T}\right)_{I=0} = -\frac{L}{G} \tag{3.34}$$

Finally, the thermal conductance k is defined as

$$k \equiv -\left(\frac{\dot{q}}{\triangle T}\right)_{I=0} = -K\left(1 + \frac{S^2GT}{K}\right) \tag{3.35}$$

Using all transmission probability of our 2 lead models in Fig 3.1,the thermoelectric coefficients are given in the Landauer-Büttiker formalism by [41, 42]

$$G = -\frac{2e^2}{h}\int_0^\infty dE \frac{\partial f}{\partial E} t(E), \tag{3.36}$$

$$L = -\frac{2e^2}{h}\frac{k_B}{e}\int_0^\infty dE \frac{\partial f}{\partial E} t(E)(E - E_F)/k_BT, \tag{3.37}$$

$$\frac{K}{T} = \frac{2e^2}{h}\left(\frac{k_B}{e}\right)^2 \int_0^\infty dE \frac{\partial f}{\partial E} t(E)\left[(E - E_F)/k_BT\right]^2, \tag{3.38}$$

where f is a Fermi function as

$$f = \left[\exp((E - E_F)/k_BT) + 1\right]^{-1}, \tag{3.39}$$

We can also compute ZT figure of merit like that

$$ZT = GS^2T/k, \tag{3.40}$$

Taking into consideration all of these calculation above, we obtain the dependence of electrical conductivity G, thermal conductance k/L_0T, the thermopower S, and ZT from the propagating modes n defined $n = \frac{2m^*E_FL^2}{\hbar^2\pi^2} - \frac{k_n^2L^2}{\pi^2}$ for stub nanowire, a ideal nanowire, and concave nanowire as Fermi function at 1K and 4K are like that ,

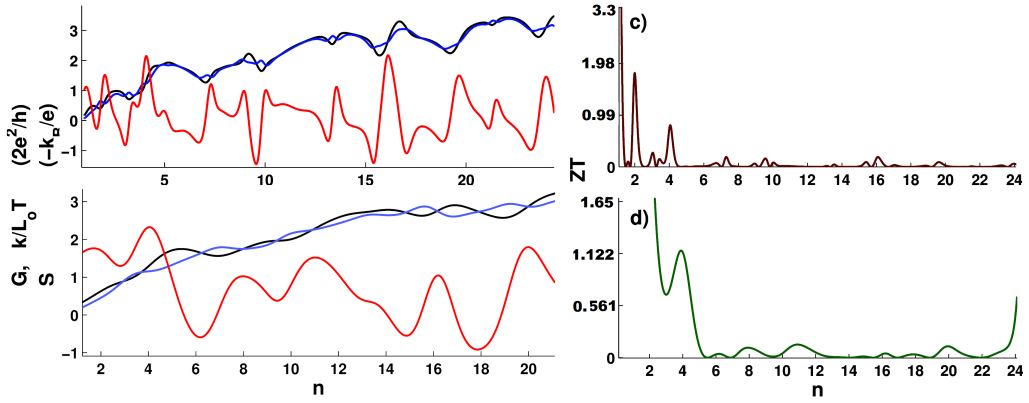

Figure 3.3: Electrical conductivity G(black curve), thermal conductance k/L_0T (blue curve), and the thermopower S (red curve) for a stub nanowire as Fermi function at (a)1K and (b)4K. The figure of merit ZT (brown curve at (c)1K, green curve at (d)4K)

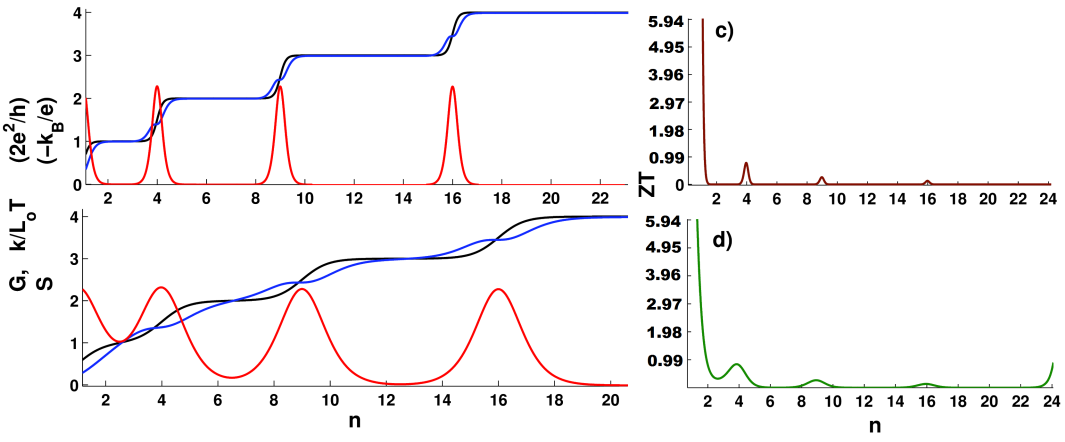

Figure 3.4: Electrical conductivity G(black curve), thermal conductance k/L_0T (blue curve), and the thermopower S (red curve) for a ideal nanowire as Fermi function at (a)1K and (b)4K. The figure of merit ZT (brown curve at (c)1K, green curve at (d)4K)

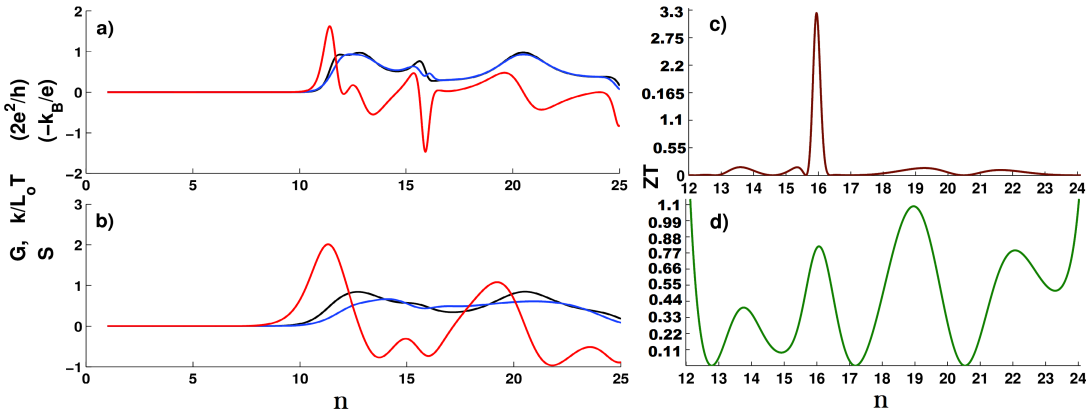

Figure 3.5: Electrical conductivity G(black curve), thermal conductance k/L_0T (blue curve), and the thermopower S (red curve) for a cavity nanowire as Fermi function at (a)1K and (b)4K. The figure of merit ZT (brown curve at (c)1K, green curve at (d)4K)

If we observe the result in figure 3.3.c), 3.4.c), 3.5.c), we will see that ZT is highest in the opening propagating modes part and when we increase temperature the number of peak of ZT curve is decreased. In figure 3.5 c), When we want to calculate ZT in cavity nanowire, it gives a meaningless result in 1^{st} and 2^{nd} opening propagating mode parts. That is why, the transmission probability of these parts must not be considered because is very near to zero in this part.

Chapter 4

Effects of inelastic scattering on thermoelectric efficiency of nanowires

This chapter which was changed a little in here, was submitted to Journal of Physics: Condensed Matter as a paper/letter on 27/06/2012.

4.1 Transmission probability in various three terminal systems

The theory acquired in chapter 3 can be extended to a system where three leads are attached to a cavity. In this chapter, in order to obtain the transmission probability for three types 3 lead system as shown in figure 4.1, we use R-matrix theory too. We show that R-matrix theory with Dirichlet boundary conditions provides a very efficient method for computing the transmission properties of the gate over a range of energies.

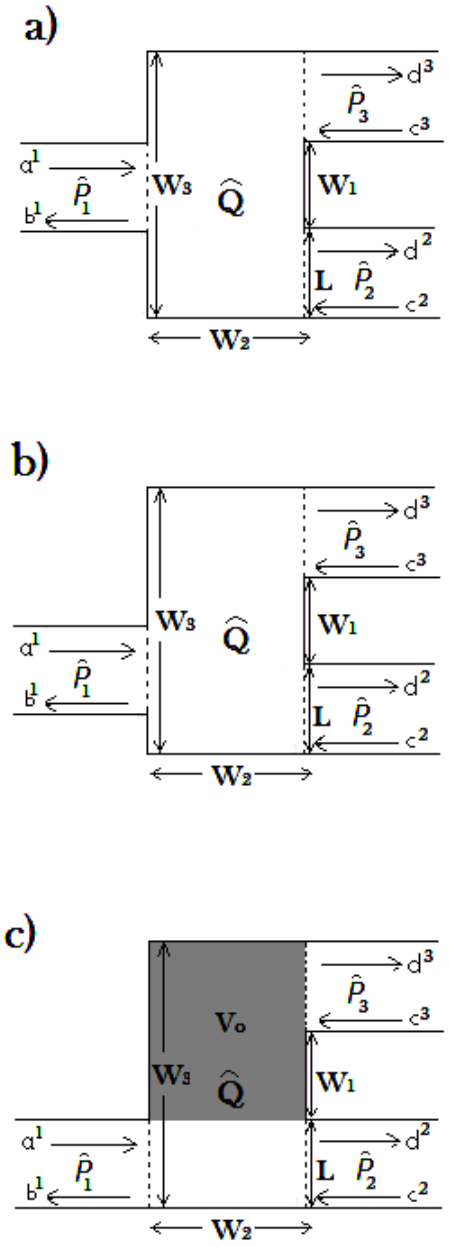

Figure 4.1: 3 lead waveguide systems

Three types 3 lead system in figure 4.1 : (a) 1^{st} type's geometry is that 1 lead in the center of left side, 2 lead in the upper and lower of right side, b) 2^{nd} type's geometry is that 1 lead move $2L/3$ to lower from center of left side, 2 lead

in the upper and lower of right side, and c) 3^{rd} type's geometry is that 1 lead move to lower end of left side, 2 lead in the upper and lower of right side,) whose transverse widths are L are separated transversally by an infinite wall whose width is W_1. The three leads are coupled by a rectangular-shaped reaction region whose longitudinal width is W_2 and transverse width is W_3. In the figure 4.1a) We want to show symmetric transmission which is transmission probability from 1^{st} lead to 2^{nd} and 3^{rd} lead are same. In the figure 4.1b), our intend is to show 1^{st} lead moving $2L/3$ to lower from center causes to breaking symmetry in the this system. In the figure 4.1c) There is a potential barrier V_0 inside the reaction region. It is our main model, because in this system we can explain easily effects of inelastic scattering on thermoelectric efficiency of nanowires and a potential barrier V_0 gradually helps us to show 3^{rd} lead's effect to our system as an inelastic scattering.

The Hamiltonian is separable in the $x-$ and $y-$ directions and this permits us to use Dirichlet boundary conditions for the entire reaction region and partially sum the expression for the $R-$matrix, because we did this procedure the preceding one section for the case of the 2 lead nanowire system.

The Schrödinger equation is satisfied by the basis states $|\psi_{p,q}\rangle$ inside the reaction region

$$\widehat{H}_{QQ}|\psi_{p,q}\rangle = E_{p,q}|\psi_{p,q}\rangle \tag{4.1}$$

where p and q are integers. We can write the eigenfunction $\langle x, y|\psi_{p,q}\rangle$ is separable as $\langle x, y|\psi_{p,q}\rangle = \phi_q(x)\Phi_p(y)$ and the eigenenergy is given by

$$E_{p,q} = \frac{\hbar^2}{2m^*}\left(\frac{p\pi}{W_2}\right)^2 + E_q^y, \tag{4.2}$$

where E_q^y is the eigenenergy of the equation

$$\left(-\frac{\hbar^2}{2m^*}\frac{d^2}{dy^2} + V(y)\right)\Phi_q(y) = E_q^y\Phi_q(y). \tag{4.3}$$

(4.3) can be solved as an expansion in sine waves, if the potential V_0 is not too strong,

$$\Phi_q(y) = \begin{cases} \sum_{m=1}^{\infty} A_m^q \sqrt{\frac{2}{W_3}} \sin\left(\frac{m\pi y}{W_3}\right) & for \quad 0 \le y \le W_3 \\ 0 & for \quad otherwise \end{cases} \tag{4.4}$$

There are three interfaces that contribute to the $R-$matrix. The indices $i = 1, 2, and \ \ 3$ used to represent functions for the three leads in figure 4.1. We can describe the electron scattering the three asymptotic regions as

$$\langle x, y|\widehat{P}_i|\psi_{p,q}\rangle = \begin{cases} \sum_{n=1}^{\infty} \chi_n^i(x) \sin\left(\frac{n\pi y}{L}\right), & i = 1 \ \ or \ \ 2 \\ \sum_{n=1}^{\infty} \chi_n^i(x) \sin\left(\frac{n\pi(y-L-W_1)}{L}\right), & i = 3 \end{cases} \tag{4.5}$$

The longitudinal wavefunction of the n^{th} propagating mode in the i^{th} waveguide is

$$\chi_n^i(x) = \begin{cases} \frac{a_n^p(i)}{\sqrt{k_n}} \exp(ik_n x) - \frac{b_n^p(i)}{\sqrt{k_n}} \exp(-ik_n x), & i = 1 \\ \frac{d_n^p(i)}{\sqrt{k_n}} \exp(ik_n x) - \frac{c_n^p(i)}{\sqrt{k_n}} \exp(-ik_n x), & i = 2 \ \ or \ \ 3 \end{cases} \tag{4.6}$$

The evanescent modes can be written in a similar manner. We have three overlap functions $u_{p,q,n}(x_i)$ that contribute to the $R-$matrix

$$u_{p,q,n}(x_i) = \sqrt{\frac{2}{L}} \int_0^L \sin\left(\frac{n\pi y}{L}\right) \psi_{p,q}(x_i, y) dy = \sqrt{\frac{2}{L}} \sin\left(\frac{n\pi x_i}{W_2}\right) f_{n,q}(i), \tag{4.7}$$

where $x_1 = 0$ and $x_2 = x_3 = W_2$,and for figure 4.1a)

$$f_{n,q}(i) = \begin{cases} \sum_{m=1}^{\infty} A_m^q \frac{2}{\sqrt{W_2 W_3}} \int_{(W_3-L)/2}^{(W_3+L)/2} \sin\left(\frac{n\pi y}{L}\right) \sin\left(\frac{m\pi y}{W_3}\right) dy, & i = 1 \\ \sum_{m=1}^{\infty} A_m^q \frac{2}{\sqrt{W_2 W_3}} \int_0^L \sin\left(\frac{n\pi y}{L}\right) \sin\left(\frac{m\pi y}{W_3}\right) dy, & i = 2 \\ \sum_{m=1}^{\infty} A_m^q \frac{2}{\sqrt{W_2 W_3}} \int_{L+W_1}^{L} \sin\left(\frac{n\pi(y-L-W_1)}{L}\right) \sin\left(\frac{m\pi y}{W_3}\right) dy, & i = 3 \end{cases} \tag{4.8}$$

for figure 4.1b)

$$f_{n,q}(i) = \begin{cases} \sum_{m=1}^{\infty} A_m^q \frac{2}{\sqrt{W_2 W_3}} \int_{(W_3-L)/2-2L/3}^{(W_3+L)/2-2L/3} \sin\left(\frac{n\pi y}{L}\right) \sin\left(\frac{m\pi y}{W_3}\right) dy, & i = 1 \\ \sum_{m=1}^{\infty} A_m^q \frac{2}{\sqrt{W_2 W_3}} \int_0^L \sin\left(\frac{n\pi y}{L}\right) \sin\left(\frac{m\pi y}{W_3}\right) dy, & i = 2 \\ \sum_{m=1}^{\infty} A_m^q \frac{2}{\sqrt{W_2 W_3}} \int_{L+W_1}^{L} \sin\left(\frac{n\pi(y-L-W_1)}{L}\right) \sin\left(\frac{m\pi y}{W_3}\right) dy, & i = 3 \end{cases} \tag{4.9}$$

for figure 4.1c)

$$f_{n,q}(i) = \begin{cases} \sum_{m=1}^{\infty} A_m^q \frac{2}{\sqrt{W_2 W_3}} \int_0^L \sin\left(\frac{n\pi y}{L}\right) \sin\left(\frac{m\pi y}{W_3}\right) dy, & i = 1 \ \ or \ \ 2 \\ \sum_{m=1}^{\infty} A_m^q \frac{2}{\sqrt{W_2 W_3}} \int_{L+W_1}^{L} \sin\left(\frac{n\pi(y-L-W_1)}{L}\right) \sin\left(\frac{m\pi y}{W_3}\right) dy, & i = 3 \end{cases} \tag{4.10}$$

where A_m^q are coefficients which are eigenvectors of relevant 1D potential barrier system. It seems that there are not any 1D potential barrier in figure 4.1 a) and b), so the eigenvectors A_m^q equals one when $m = q$, equals zero when $m \neq q$, and in figure 4.1 c), the A_m^q eigenvectors of relevant potential barrier system are obtained owing to solving 1D barrier system problem. In addition I would like to specify we use $V_0 \tanh 40(x - W_3/3)/W_3$ instead of V_0, in order to avoid a Gibbs phenomenon. These following changes have very little effect to our transmission probability.

Next, with using trigonometric series (3.20),(3.21) [39], we obtain the $R-$ matrix elements as follows

$$
\begin{aligned}
R_{11}(n,n') &= \sum_{q=1}^{\infty} f_{q,n}(1) f_{q,n'}(1) k_q csc(k_q W_2) cos(k_q W_2), \\
R_{12}(n,n') &= \sum_{q=1}^{\infty} f_{q,n}(1) f_{q,n'}(2) k_q csc(k_q W_2), \\
R_{13}(n,n') &= \sum_{q=1}^{\infty} f_{q,n}(1) f_{q,n'}(3) k_q csc(k_q W_2), \\
R_{21}(n,n') &= \sum_{q=1}^{\infty} f_{q,n}(2) f_{q,n'}(1) k_q csc(k_q W_2), \\
R_{22}(n,n') &= \sum_{q=1}^{\infty} f_{q,n}(2) f_{q,n'}(2) k_q csc(k_q W_2) cos(k_q W_2), \\
R_{23}(n,n') &= \sum_{q=1}^{\infty} f_{q,n}(2) f_{q,n'}(3) k_q csc(k_q W_2) cos(k_q W_2), \\
R_{31}(n,n') &= \sum_{q=1}^{\infty} f_{q,n}(3) f_{q,n'}(1) k_q csc(k_q W_2), \\
R_{32}(n,n') &= \sum_{q=1}^{\infty} f_{q,n}(3) f_{q,n'}(2) k_q csc(k_q W_2) cos(k_q W_2), \\
R_{33}(n,n') &= \sum_{q=1}^{\infty} f_{q,n}(3) f_{q,n'}(3) k_q csc(k_q W_2) cos(k_q W_2)
\end{aligned}
\tag{4.11}
$$

where $k_q = \sqrt{\frac{2m^*E}{\hbar^2} - E_q^y}$. Note that (4.11) holds when $\frac{2m^*E}{\hbar^2} > E_q^y$.By the way, E_q^y is eigenvalue of relevant three lead systems.

$$
R_{11} = \sum_{q=1}^{\infty} f_{q,n}(1) f_{q,n'}(1) \widetilde{k}_q csch(\widetilde{k}_q W_2) cosh \widetilde{k}_q W_2),
$$

$$
\begin{aligned}
R_{12} &= \sum_{q=1}^{\infty} f_{q,n}(1) f_{q,n'}(2) \widetilde{k}_q csch(\widetilde{k}_q W_2), \\
R_{13} &= \sum_{q=1}^{\infty} f_{q,n}(1) f_{q,n'}(3) \widetilde{k}_q csch(\widetilde{k}_q W_2), \\
R_{21} &= \sum_{q=1}^{\infty} f_{q,n}(2) f_{q,n'}(1) \widetilde{k}_q csch(\widetilde{k}_q W_2), \\
R_{22} &= \sum_{q=1}^{\infty} f_{q,n}(2) f_{q,n'}(2) \widetilde{k}_q csch(\widetilde{k}_q W_2) cosh(\widetilde{k}_q W_2), \\
R_{23} &= \sum_{q=1}^{\infty} f_{q,n}(2) f_{q,n'}(3) \widetilde{k}_q csch(\widetilde{k}_q W_2) cosh(\widetilde{k}_q W_2), \\
R_{31} &= \sum_{q=1}^{\infty} f_{q,n}(3) f_{q,n'}(1) \widetilde{k}_q csch(\widetilde{k}_q W_2), \\
R_{32} &= \sum_{q=1}^{\infty} f_{q,n}(3) f_{q,n'}(2) \widetilde{k}_q csch(\widetilde{k}_q W_2) cosh(\widetilde{k}_q W_2), \\
R_{33} &= \sum_{q=1}^{\infty} f_{q,n}(3) f_{q,n'}(3) \widetilde{k_q} csch(\widetilde{k}_q W_2) cosh(\widetilde{k}_q W_2)
\end{aligned}
\tag{4.12}
$$

Note that (4.12) holds when $\frac{2m^* E}{\hbar^2} < E_q^y$, $k_q \rightarrow i\widetilde{k}_q$, $\widetilde{k}_q = \sqrt{E_q^y - \frac{2m^* E}{\hbar^2}}$, $\sin k_q x \rightarrow i \sinh \widetilde{k}_q x$ and $\cos k_q x \rightarrow \cosh \widetilde{k}_q x$.

For the 3 lead system, the sub-matrix of the $R-$ matrix, $\mathbf{R_{PP}}$, consists of 9 sub-matrices such that

$$
\mathbf{R_{PP}} = \begin{pmatrix} R_{11}(p,p) & R_{12}(p,p) & R_{13}(p,p) \\ R_{21}(p,p) & R_{22}(p,p) & R_{23}(p,p) \\ R_{31}(p,p) & R_{32}(p,p) & R_{33}(p,p) \end{pmatrix} \tag{4.13}
$$

The matrix $\mathbf{R_{PP}}$ is a $3N_P \times 3N_P$ matrix. The matrices $\mathbf{R_{PE}}$, $\mathbf{R_{EP}}$ and $\mathbf{R_{EE}}$ can also be formed in a similar manner.

The $S-$matrix relates all the incomingwaves to all the outgoingwaves. Using the continuity of the first derivative of the wavefunctions at the interfaces gives us an S-matrix in a manner similar to that used to obtain the S-matrix for preceding one section for the case of the 2 lead nanowire system,

$$\begin{pmatrix} b^1 \\ d^2 \\ d^3 \end{pmatrix} = \begin{pmatrix} S_{11} & S_{12} & S_{13} \\ S_{21} & S_{22} & S_{23} \\ S_{31} & S_{32} & S_{33} \end{pmatrix} \cdot \begin{pmatrix} a^1 \\ c^2 \\ c^3 \end{pmatrix} \tag{4.14}$$

In numerical calculations, we assume that an electron enters into the cavity only from nanowire $i = 1$, so that $(a^1, c^2, c^3)^T = (1, 0, 0)^T$. The total transmission probability is given by

$$T = \sum_{m=1}^{N_P} \sum_{n=1}^{N_P} |(S_{r,l})_{nm}|^2 \tag{4.15}$$

Since the wave function along the transversal direction in the leads is quantized, the 1^{st} propagating mode opens at $E_n = \frac{\hbar^2}{2m*} \left(\frac{n\pi}{L}\right)^2$. Owing to scale invariance, all units are scaled with the width of lead 1, w_1 in figure 4.1. Energy unit for instance is given as $E_1 = (\hbar^2/2m*)(\pi/w_1^2) = 0.0753eV$ for $w_1 = 2\pi/5$ lead where we used effective mass $m* = 0.05m_e$. There are several possible parameters to change, we fix non essential ones for the sake of firm description. For this reason, we fixed the geometry of our model with the following parameters, $w_1 = 2\pi/5$, $w_2 = \pi$, $w_3 = 6\pi/5$, all leads have same width $L = 2\pi/5$. Taking into consideration all of them are shown above, we obtained each transmission probability of a model shown in figure 4.1. Some of these transmission probability (T_{12},T_{13},T_{23}) for each model of figure 4.2, 4.3, 4.4, 4.5, 4.6, 4.7 are shown below.

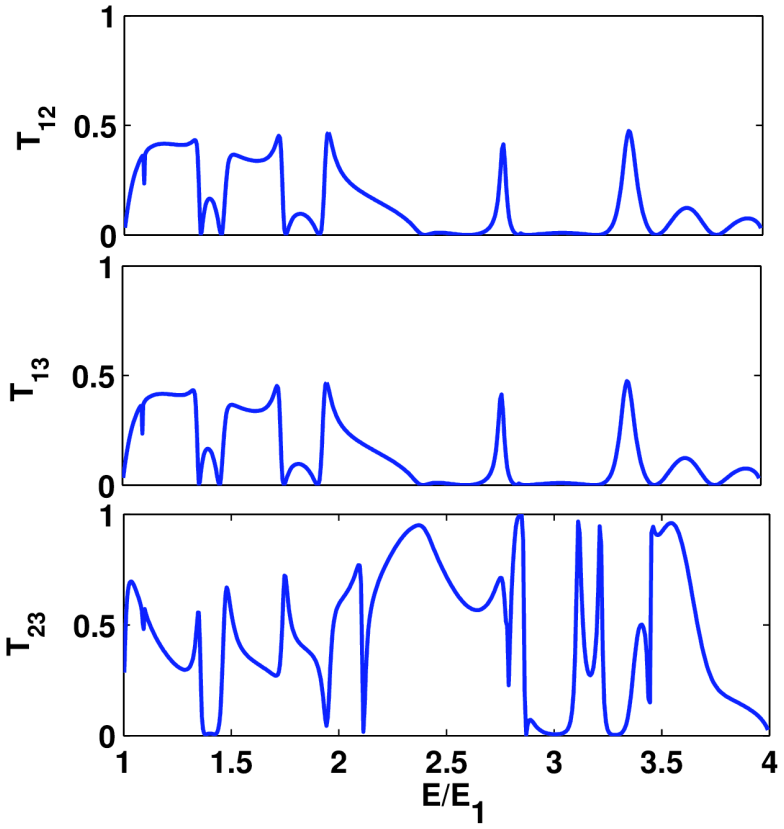

Figure 4.2: Transmissions probability in the symmetric three lead system a) T_{12}, b) T_{13}, c) T_{23}.

In the symmetric three terminal system, the transmission probability T_{12} and T_{13} are the same. Symmetric three terminal system is applicable for controlling the heat flux [20].

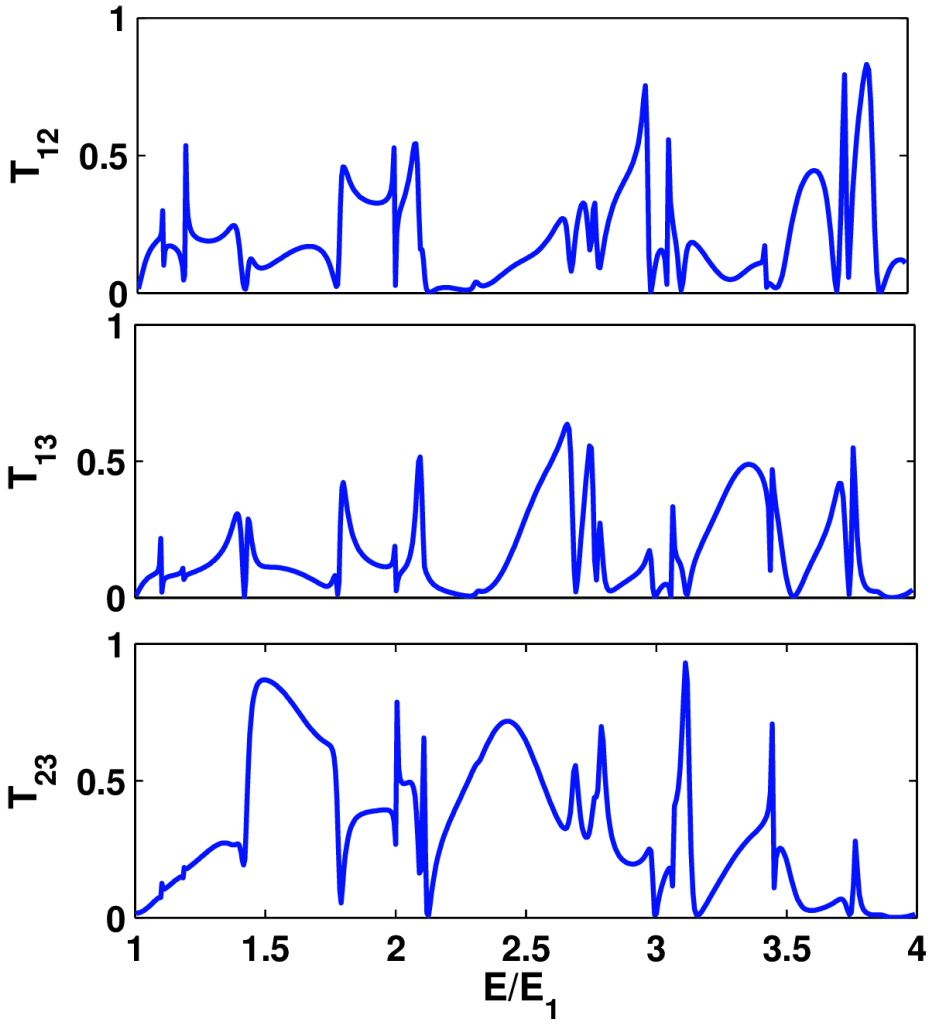

Figure 4.3: Transmissions in the third lead which 1^{st} lead slide the lever down in figure 4.1(b). a) T_{12}, b) T_{13}, c) T_{23}.

In figure 4.3, we slide 1^{st} lead move $2L/3$ to lower from center which this proses causes antisymmetric three terminal system , and we observe that the transmission probability T_{12} and T_{13} are different.

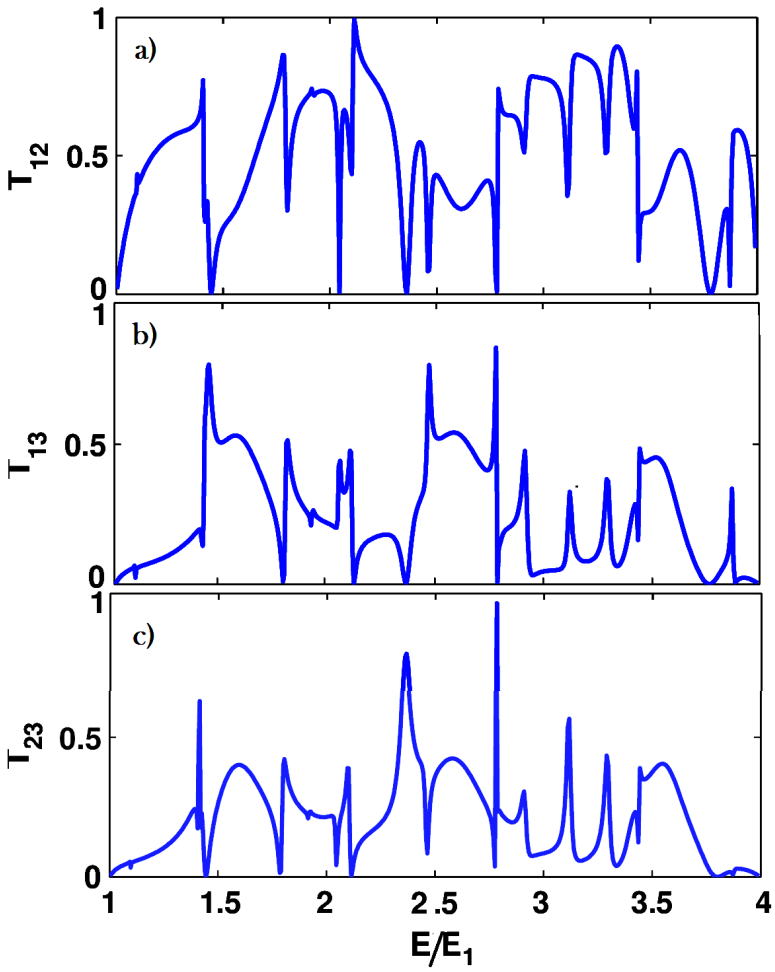

Figure 4.4: Transmissions in the case of no potential barrier exists in the third lead. a)T_{12}, b)T_{13}, c) T_{23}.

In our research work, we utilise the results of figure 4.1c) model shown figure 4.4, 4.5, 4.6, 4.7 . The reason is the results of figure 4.1c) model is that these results are a more convenient to explain a effects of inelastic scattering on thermoelectric efficiency of nanowires.

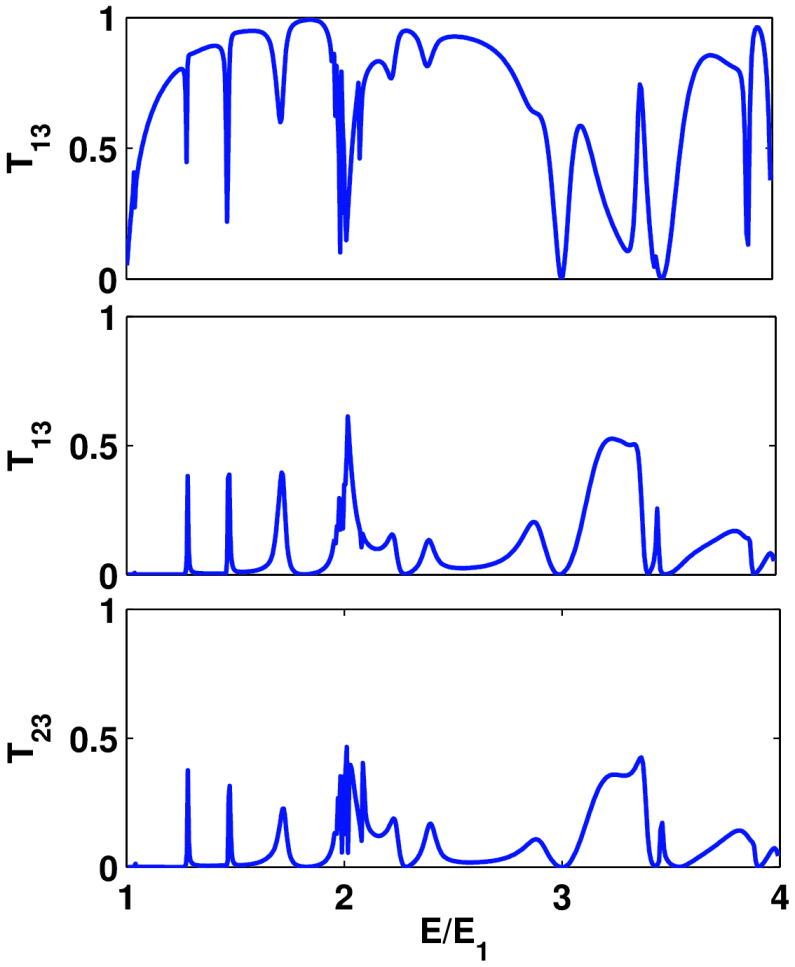

Figure 4.5: Transmissions in the case of $5E_1$ potential barrier exists in the third lead. a) T_{12}, b) T_{13}, c) T_{23}.

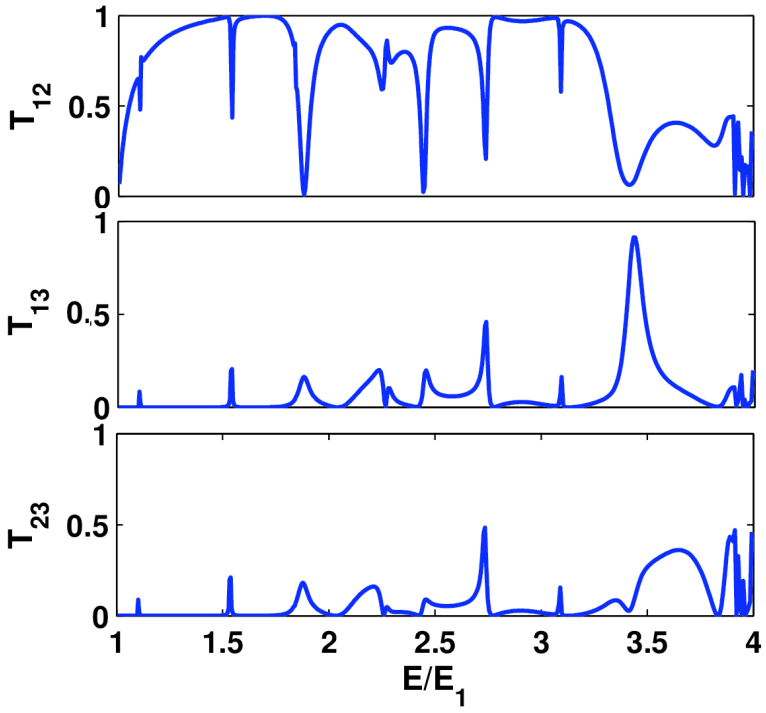

Figure 4.6: Transmissions in the case of $20E_1$ potential barrier exists in the third lead. a) T_{12}, b) T_{13}, c) T_{23}.

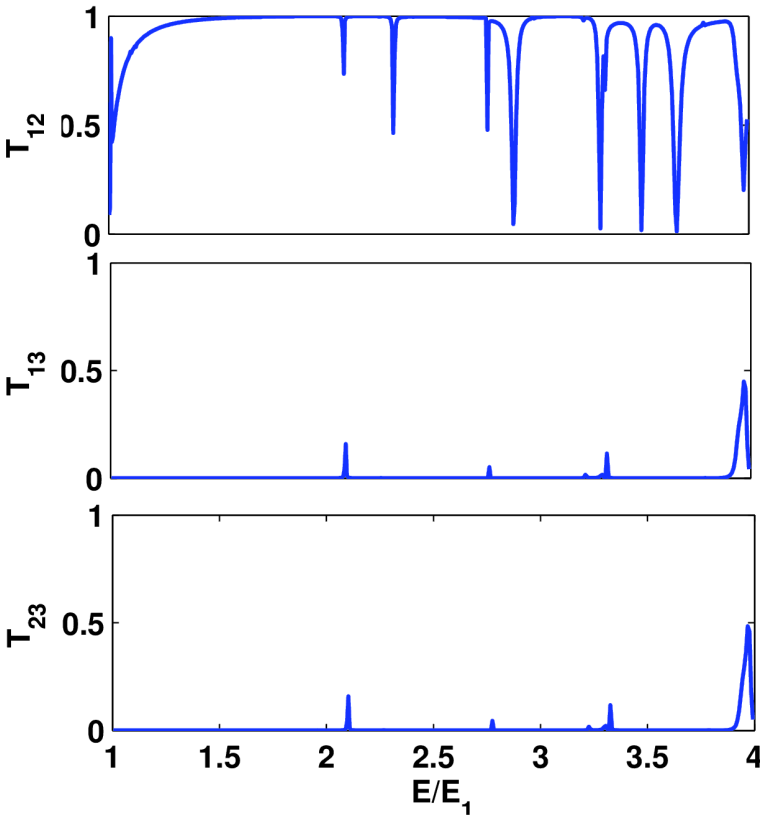

Figure 4.7: Transmissions in the case of $100E_1$ potential barrier exists in the third lead. a) T_{12}, b) T_{13}, c) T_{23}.

4.2 Model System

We use a Landauer-Buttiker approach in our model for inelastic scattering. A schematic of the model nanowire is presented in Fig. 4.8. A perfect nanowire between two reservoirs is connected in the middle to a third probe lead with its own reservoir as sketched in Fig. 4.8. This third reservoir is either constant temperature (isotropic) and a varying potential V_p such that the zero current in the probe lead or both varying temperature (adiabatic) and potential such that both current and heat drawn are constant in probe lead. The probe lead models the inelastic scattering. In other words, we effectively exchange coherent electrons with incoherent ones coming from the third reservoir while keeping the current

zero. We change the strength of inelastic scattering by controlling a coupling parameter in the form of a constant potential just beyond the contact of the probe lead to the nanowire (dark grey region in Fig. 4.8).

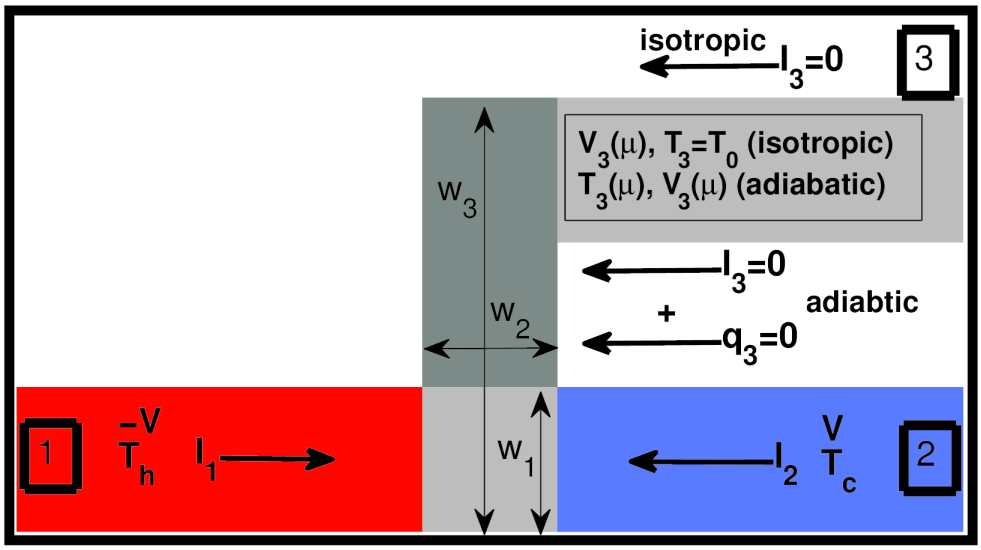

Figure 4.8: The model of the quantum wire with hot (left-red), cold (right-blue) and probe (middle-gray) reservoirs. In all calculations, $V_1 = -V$, $V_2 = +V$, $\theta_1 = 0.06E_1/k_B$, and $\theta_2 = 0.04E_1/k_B$ are used. The probe voltage and temperature are found depending on the kind of process. A potential barrier has been included in dark gray region in probe lead in some calculations.

The two dimensional Schrödinger equation for the geometry described in Fig. 4.8 is solved using the reaction matrix theory [25, 27]. The total Hamiltonian of the system is projected into lead and scattering regions with singular coupling at the interface of these regions. Note that the condition on the projection is keeping the total Hamiltonian of the system as a Hermitian conjugate. Assuming a known solution in the leads' scattering region is expanded into a discrete set of basis function obtained by assuming a fixed boundary condition on the interface. In an integrable geometry formed from rectangular regions, the bases states formed from Dirichlet boundary condition at the interface seems to

give the best results. The main reason is that we were able to include the infinite summation exactly into the expansion of wave function in scattering region along the longitudinal direction of the nanowire.

We have the transmission amplitudes of the system shown in Fig. 4.8 after solving the Schrödinger equation. We report our results without referring to a specific system. For example, we present energy in terms of E_1 including thermal energy whenever it is possible. Since, there are several possible parameters to change, we fix non essential ones for the sake of firm description. For this reason, we fixed the geometry of our model with the following parameters, $w_1 = 2\pi/5$, $w_2 = \pi$, $w_3 = 6\pi/5$, all leads have same width, and we have $k_B\theta_h = 0.06E_1$ for the lead 1, and we have $k_B\theta_c = 0.04E_1$ for lead 2, where k_B is the Boltzman constant $k_B = 8.6e^{-5}ev/K$ and θ is temperature.

In Fig 4.4, 4.5, 4.6, 4.7, we present some of the transmission probabilities for the geometry displayed in Fig. 4.8 when the third lead is fully open to the nanowire, i.e. no potential barrier, when there is $5E_1$ potential barrier in the third lead,when there is $20E_1$ potential barrier in the third lead,when there is $100E_1$ potential barrier in the third lead. Putting the various potential barrier beyond the interface of nanowire and third lead cause the constriction of the exposition of third lead . By increasing this potential, the third lead will effectively detach from the nanowire, and the system will return back to the perfect nanowire condition. The transmission probabilities to the third lead, T_{13} and T_{23}, effectively become zero in this case. The conductance is defined in terms of transmission probability, $G_{\alpha,\beta} = (2e^2/h^2)T_{\alpha,\beta}$, which determines all thermoelectric properties of the system at hand. We limit our calculation to the case when there is one open channel in each lead where the effect of inelastic scattering on its thermoelectric properties is at the highest. We have nine transmission probabilities for the three lead system, however not all of them are independent because of the time reversal symmetry, but obeys the following relation

$$\sum_{\alpha} T_{\alpha,\beta} = \sum_{\beta} T_{\alpha,\beta} \tag{4.16}$$

as well as for each of the transmissions,$T_{\alpha,\beta} = T_{\beta,\alpha}$. This can also be explained in terms of flux conservation, that is, if each lead is connected to the same reservoirs,

the total current should be zero.

The current in each lead as shown in Fig. 4.8 is given in terms of the conductance as

$$I_\alpha = \sum_{\beta\neq\alpha} \frac{\hbar}{e}(G_{\alpha,\beta}V_\alpha - G_{\beta,\alpha}V_\beta) \tag{4.17}$$

for the case when the temperature is zero, $\theta = 0$K. When the temperature of the reservoirs is different than zero, $\theta \neq 0$K, we have,

$$I_\alpha = \sum_{\beta\neq\alpha} \frac{2e}{h} \int dE(T_{\alpha,\beta}(E)f_\alpha(E,V,\theta) - T_{\beta,\alpha}(E)f_\beta(E,V,\theta)) \tag{4.18}$$

where the Fermi distribution is given by

$$f_\alpha(E,V,\theta) = \frac{1}{1+\exp(\frac{E-\mu_\alpha}{k_B\theta})}, \tag{4.19}$$

where $\mu_\alpha = \mu + V_\alpha$ is the chemical potential of each lead for a given average chemical potential μ which can be adjusted with back gates to the appropriate energy and V_α is the bias on each leads as shown in Fig. 4.8. The heat extraction rate for each lead is given by

$$\dot{q}_\alpha = \sum_{\beta\neq\alpha} \frac{2}{h} \int dE((E-\mu_\alpha)T_{\alpha,\beta}(E)f_\alpha(E,V,\theta) - (E-\mu_\beta)T_{\beta,\alpha}(E)f_\beta(E,V,\theta)). \tag{4.20}$$

We will use the current and heat extraction rate to define power and efficiency in the nonlinear response theory. First, we present a linear response theory for inelastic scattering.

4.3 Linear Response Theory

When the temperature difference and the bias are very close to each other, it is possible to expand Fermi energy in Taylor series and approximate both the current and the heat extraction rate in terms of one bias and temperature parameter. In the linear response regime, we have

$$\begin{aligned} I_\alpha &= \sum_\beta G_{\alpha\beta}\Delta V_\beta + \sum_\beta S_{\alpha\beta}G_{\alpha\beta}\Delta\theta_\beta, \\ \dot{q}_\alpha &= -\sum_\beta \theta S_{\alpha\beta}G_{\alpha\beta}\Delta V_\beta - \sum_\beta \kappa_{\alpha\beta}\Delta\theta_\beta \end{aligned} \tag{4.21}$$

where $\Delta\theta_\beta$ is the temperature difference between the contacts α and β, G is the electric conductance, κ is the heat conductance, S is the Seeback coefficient, and θ is the temperature. The transport coefficients in the Landauer-Buttiker formulation are expressed as follows

$$G_{\alpha,\beta} = \frac{2e^2}{h}\int_0^\infty dE \frac{\partial f}{\partial E}(N_\alpha \delta_{\alpha,\beta} - T_{\alpha,\beta}(E)) \tag{4.22}$$

$$S_{\alpha,\beta} = \frac{1}{G_{\alpha\beta}}\frac{2e^2}{h}\frac{k_B}{e}\int_0^\infty dE \frac{\partial f}{\partial E}((N_\alpha \delta_{\alpha,\beta} - T_{\alpha,\beta}(E))(E-\mu)/k_B\theta \tag{4.23}$$

$$\frac{K_{\alpha,\beta}}{\theta} = \frac{2e^2}{h}(\frac{k_B}{e})^2\int_0^\infty dE \frac{\partial f}{\partial E}((N_\alpha \delta_{\alpha,\beta} - T_{\alpha,\beta}(E))[(E-\mu)/k_B\theta]^2 \tag{4.24}$$

where we have N_α channel open in lead α and heat conduction is related to $K_{\alpha\beta}$ via $\kappa_{\alpha\beta} = -K_{\alpha\beta}(1 + S^2_{\alpha\beta}G_{\alpha\beta}\theta/K_{\alpha\beta})$. The derivative of the Fermi function with respect to energy is near $V_\alpha = \theta_\alpha = 0$. In the linear response theory, we can calculate all quantities for the electronic figure of merit, $ZT = GTS^2/\kappa$ and corresponding efficiency

$$\eta_{max} = \eta_C \frac{\sqrt{ZT+1}-1}{\sqrt{ZT+1}+1} \tag{4.25}$$

hence the Carnot limit, η_C, is reached when $ZT \to \infty$. Adding a third lead changes conductance in a way in which it is possible to extract work in a wide range of energy. Next, we briefly deliberate the meaning of adding a third lead to the nanowire, before discussing the results of the linear response and nonlinear response calculations.

4.4 Inelastic scattering

We demonstrate how this model describes the inelastic scattering process by examining the simplest case where the temperature is set zero. Note that in Fig. 4.8, the third lead is the probe lead. The current for this lead is made zero by allowing an appropriate bias formed in the reservoir that this lead is connected to, so we have

$$I_3 = 0 = V_3(T_{13} + T_{23}) - (V_1T_{13} + V_2T_{23}) \tag{4.26}$$

from which we obtain,

$$V_3 = \frac{V_1 T_{13} + V_2 T_{23}}{T_{13} + T_{23}}. \tag{4.27}$$

Since the sum of all currents should be zero, we have the condition $I_1 = -I_2$. Hence, we can write the current in nanowire after substituting V_3 as

$$I_1 = \frac{e}{h}(T_{12} + \frac{T_{13}T_{23}}{T_{13} + T_{23}})(V_1 - V_2). \tag{4.28}$$

This current is similar to the perfect nanowire with zero temperature case apart from the extra term coming from the probe lead. When we set the current to zero, we exchange particles with the third reservoir while keeping total energy constant in the nanowire. In this way, we replace coherent electrons with incoherent ones. Though, it is simple to demonstrate inelastic scattering for zero temperature, with nonlinear temperature difference and high bias, we have more complicated equations, and so a numerical solution would be necessary for the general case.

4.5 Isotropic and Adiabatic Process

The probe lead in Fig. 4.8 (i.e. lead 3) is in contact with a reservoir isotropically or adiabatically in our calculations. For the isotropic condition, we set the temperature of this lead to a constant value, $\theta = 0.05E_1/k_B$, while the temperature of the hot (lead 1) and cold (lead 2) are $\theta = 0.06E_1/k_B$ and $\theta = 0.04E_1/k_B$, respectively. Next, we look at the condition for zero current $I_3 = 0$.

In the linear response, we use Eq. 4.21 to write the current in the probe lead and find the bias required to make the current zero, which is

$$V_3 = \frac{G_{31}V_1 + G_{32}V_2}{G_{31} + G_{32}} + \frac{S_{31}G_{31}}{G_{31} + G_{32}}(\theta_1 - \theta_3) + \frac{S_{32}G_{32}}{G_{31} + G_{32}}(\theta_2 - \theta_3). \tag{4.29}$$

The current in the nanowire is now determined as we discussed in the zero temperature case, i.e. we substitute V_3 in I_1, so

$$I = gV_{12} + S_{12}G_{12}\theta_{12} + S_{13}G_{13}\theta_{13} - \frac{G_{13}}{G_{31} + G_{32}}[S_{13}G_{13}\theta_{13} + S_{32}G_{32}\theta_{32}] \tag{4.30}$$

where $-g = G_{12} + G_{13}G_{32}/(G_{31} + G_{32})$ is the conductance as in the zero temperature case. Then, we can get thermopower from the known current in the

nanowire from the definition of thermopower, which is

$$S_{tp} \equiv \frac{\Delta V}{\Delta \theta}|_{I=0} \tag{4.31}$$

When we set the current equal zero, we obtain the required relation for thermopower. [24]

$$S_{tp} = -\frac{1}{g}\left(S_{12}G_{12} + \frac{1}{2}S_{13}G_{13} + \frac{1}{2}\frac{G_{13}}{G_{31}+G_{32}}(S_{32}G_{32} - S_{31}G_{31})\right) \tag{4.32}$$

where we use $\Delta V = V_1 - V_2$ and $\theta_3 = (\theta_1 + \theta_2)/2$. Note that we recover the zero inelastic case result at which thermopower is equivalent to the Seeback coefficient.

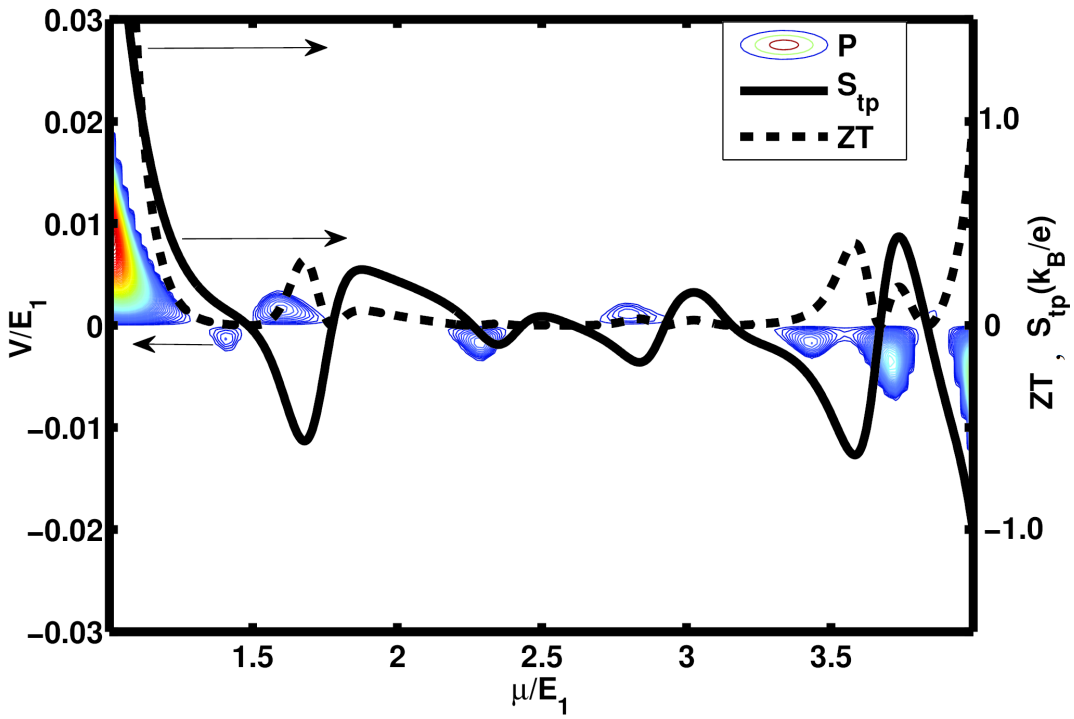

Figure 4.9: Power, thermopower (S_{tp}), and figure of merit (ZT) of a nanowire in the case of isotropic process. Scale difference indicated by the arrows as shown. The left axis shows bias for the power, and the right axis represents the thermopower and ZT. Thermopower has units of k_B/e and ZT is unitless.

We find the current without using linear response approximation as well. First, we find the zero of the equations for each chemical potential μ,

$$I_3 = \frac{2e}{h}\int dE(T_{31}(f_3 - f_1) + T_{32}(f_3 - f_2)) \tag{4.33}$$

which gives the numerical value of $V_3(\mu)$. Next, we substitute this in the relation for I_1, which is

$$I_1 = \frac{2e}{h} \int dE(T_{12}(f_1 - f_2) + T_{13}(f_1 - f_3), \tag{4.34}$$

to find the current in the nanowire modified by the probe. Power is defined as $P = I\Delta V$. The power calculated with this approach is shown in Fig. 4.9. We also present the linear response result for the isotropic case as well as ZT in the same plot. As seen in Fig. 4.9, there is a strong correlation between thermal power and the total power extracted from the nanowire.

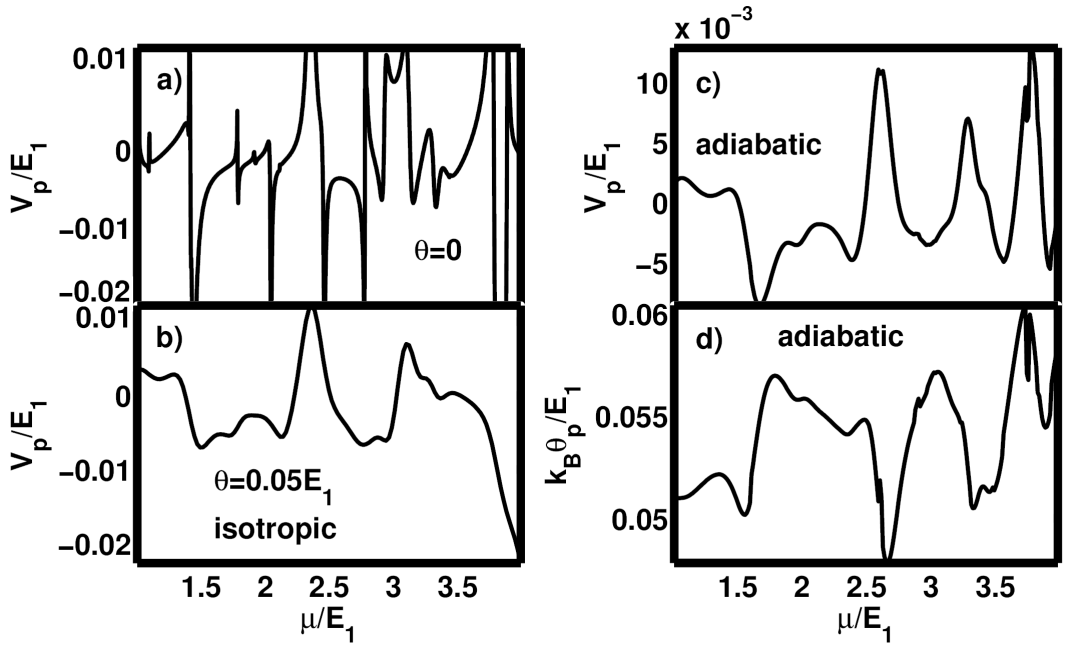

Figure 4.10: a) Potential bias measured on the third lead versus chemical potential when temperature is zero in each lead. b) Potential bias on the third lead for an isotropic process where temperature is set to $k_B\theta = 0.05E_1$ in probe lead. c) Potential bias and d) temperature on the third lead versus chemical potential for an adiabatic process.

In adiabatic process, we require the current as well as heat current to be set to zero in the probe lead. This can be done in a similar fashion, and we refer for the explicit expression of the linear response calculation for thermopower

to reference [24]. We used nonlinear response for this case as well. We self consistently solve the equations for current and heat current.

$$I_3 = \frac{2e}{h}\int dE(T_{31}(f_3 - f_1) + T_{32}(f_3 - f_2)$$
$$\dot{q}_3 = \frac{2e}{h}\int dE(T_{31}(E-\mu_3)(f_3 - f_1) + T_{32}(E-\mu_3)(f_3 - f_2) \tag{4.35}$$

where $\mu_3 = \mu + V_3$. In order to find the zero of this equation system, we first find V_3 from the current expression and use it to find θ_3, and then iterate on this procedure.

In Fig. 4.10, we present probe voltage and temperature for various processes. While we display the zero temperature case using equation 4.27 in Fig. 4.10a, we demonstrate the isotropic case with temperature $\theta = 0.05E_1/k_B$ and V_p calculated from nonlinear equation 4.33 in Fig. 4.10b. In Fig. 4.10c and Fig. 4.10d, we plot self consistent probe voltage and temperature calculated from Eq. 4.35 for the adiabatic case. In all cases in Fig. 4.10, we use $V_1 = -0.03$, $V_2 = 0.03$, $k_B\theta_1 = 0.06E_1$, and $k_B\theta_2 = 0.04E_1$.

We note that there is not much difference between the thermopower of isotropic and adiabatic cases for the range of paramaters we use the in linear response regime (not shown). We discuss the efficiency of the nanowire as a heat engine in the following section.

4.6 Efficiency at Maximum Power

We treat the Fermi energy without any approximation in the nonlinear response. We find the power and the efficiency with the following definitions

$$P = I\Delta V \ , \eta = \frac{P}{\dot{q}_1} \tag{4.36}$$

where the heat is extracted from the hot reservoir. We change the bias and the chemical potential to investigate the power and the efficiency.

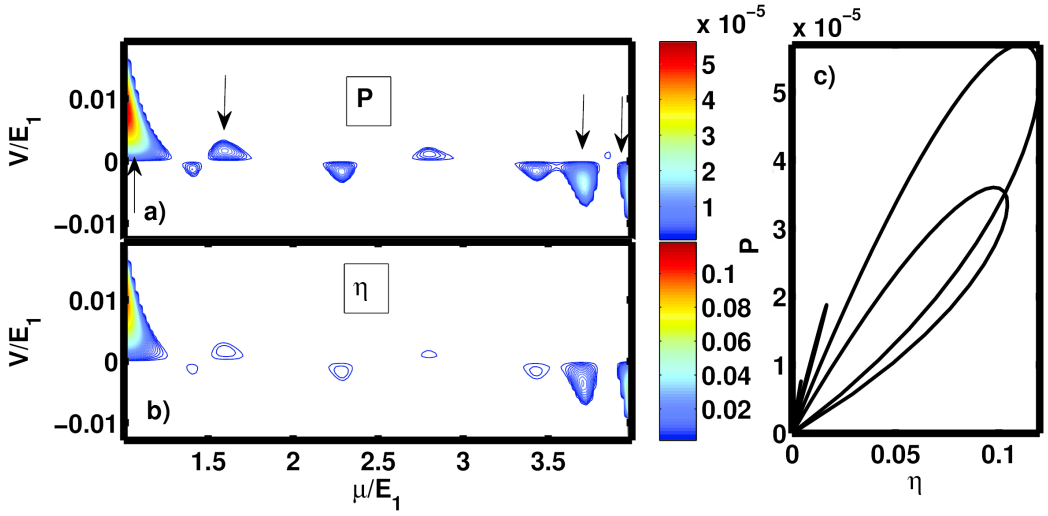

Figure 4.11: a) Power extracted when there is no current on the probe lead, b) efficiency with respect to chemical potential and bias change.c) Loop diagrams of power versus efficiency obtained by keeping the chemical potential constant at the points marked with arrows in a).

In Fig. 4.11, we show these quantities for the system depicted in Fig. 4.8 with no barrier potential. Power is shown in Fig. 4.11a. We only plot positive power extracted from the heat engine for the given temperature difference.

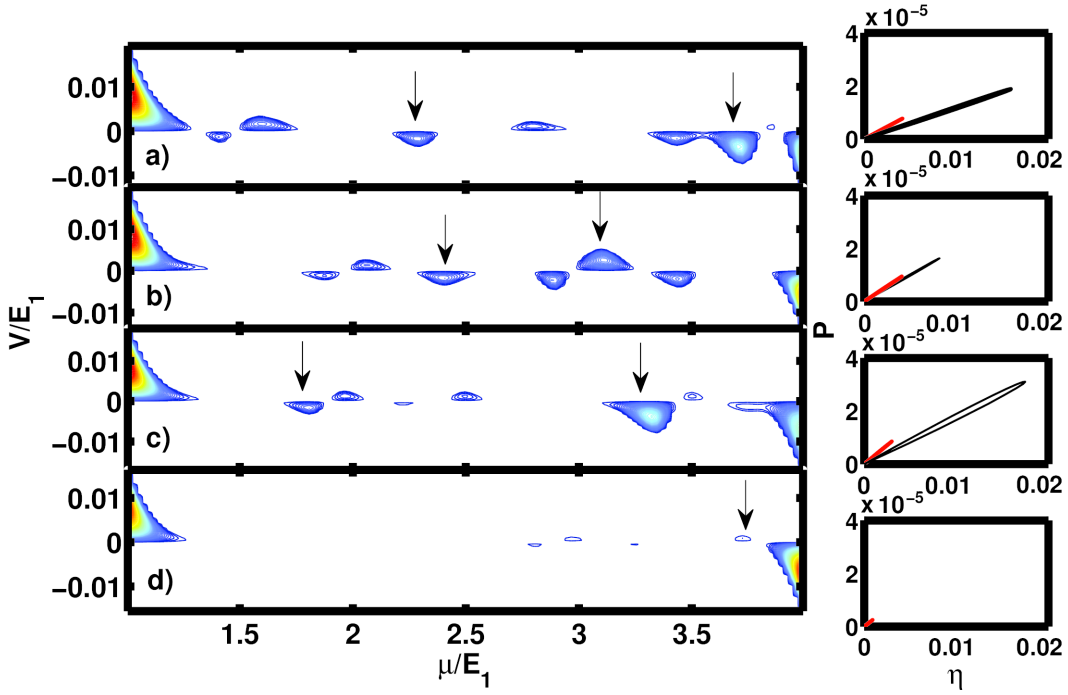

Figure 4.12: Power output by the strength of inelastic scattering increasing from top to bottom. a) $V_{barr} = 0$, b) $V_{barr} = 5E_1$, c) $V_{barr} = 20E_1$, and d) $V_{barr} = 100E_1$.

In Fig. 4.11b, we present the efficiency for the same parameters. In Fig. 4.11c, we demonstrate the loop diagram to show the efficiency at the max power. The chemical potential for each loop is chosen such that power has a maximum, and is kept constant on that value. We see that there are a multitude of regions in energy for which this system can be used as a heat engine. However, the efficiency is quite low for the places other than channel openings.

In Fig. 4.12, we discuss the effect of the strength of inelastic scattering on the performance of the nanowire heat engine. The potential barrier, V_{barr}, we introduced at the connection of the probe lead to the nanowire (dark gray region) shown in Fig. 4.8 has an effect on the power output. With increasing barrier potential ($V_{barr} = 0$ in Fig. 4.12a, $V_{barr} = 5E_1$ in Fig. 4.12b, $V_{barr} = 20E_1$ in Fig. 4.12c, and $V_{barr} = 100E_1$ in Fig. 4.12d), we observe a decrease of regions which can be used as a heat engine. In the inset to each figure, we also show

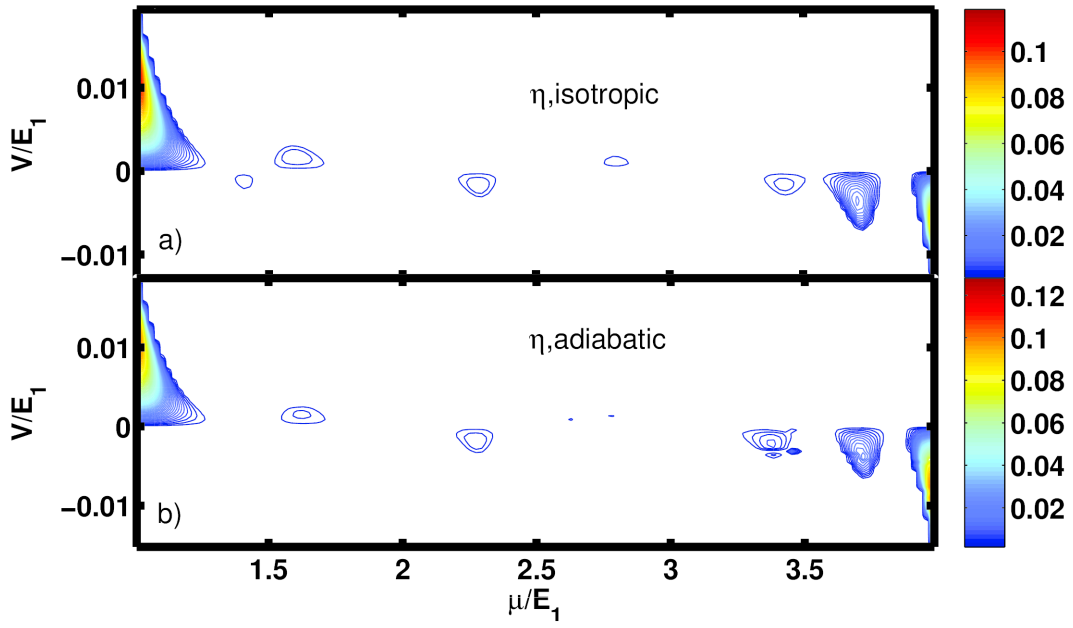

Figure 4.13: a) Efficiency of the isotropic process, b) efficiency of the adiabatic process.

the loop diagrams for the next two highest power outputs other than the channel opening ones. We also observe shifts in the position of power output regions in energy with the changing strength of the inelastic scattering.

In Fig. 4.13, we show the effect of the isotropic process and the adiabatic process on the efficiency. As seen in Fig. 4.13a, we calculate the efficiency by assuming a constant temperature in the probe lead. In Fig. 4.13b, we present the efficiency for the adiabatic case where the probe lead temperature and the voltage are set according to the condition of zero current and zero heat extraction. As in the linear response theory, we do not see much difference here. We conclude that the efficiency is not strongly dependent on the process of the probe lead, at least for the parameters we used.

Chapter 5

Conclusion

In this thesis, initially, electron transmission in three type 2 lead nanowires is investigated in terms of R-matrix method. Next, these transmission probabilities of their system are applied to Landauer-Büttiker formalism to know how their geometries effect to conductance G, the thermopower S, the figure of merit ZT.

The effect of inelastic scattering on the performance of a nanowire heat engine using the linear response and nonlinear response theories is investigated. The regions of energy where the nanowire can be used as heat engine increases as the strength of inelastic scattering also increases. We obtain non-zero efficiencies owing to inelastic scattering where the efficiency of a perfect nanowire as a heat engine is expected to be zero at these energies. Showing the linear response results indeed capture some of the features of the nonlinear response analysis. Besides, the feasibility of a nanowire as a heat engine is only found from the nonlinear response calculations, since the linear response theory gives no details about the process' time and power.

We have not discussed the effect of geometry and temperature bias in this work, assuming the geometry will only change the amount of inelastic scattering and temperature bias is similar to potential bias. We parameterize the amount of the inelastic scattering by using a potential barrier in the probe lead. It is possible to attach a probe wider than the width of the nanowire to change the

amount of inelastic scattering, but this may bring about some problems with vertical currents in the lead, invalidating the assumptions on the probe lead [43]. We assume a perfect nanowire to show the effects clearly. The inelastic scattering model helps to understand some kinds of interaction which is the effect of electron-electron interaction, as well as phonon drag were qualitatively discussed in the reference [13] on the efficiency of the nanowire heat engine as long as the strength of coupling is known. Looking at a rough nanowire with the same methods involves no technical difficulty. The efficiencies calculated here are also based only on the electronic part of the transport. The phononic part further reduces total efficiency. The total figure of merit ZT' is given as a fraction of electronic ZT, such as $ZT' = ZT(\kappa_p/(\kappa_e + \kappa_p))$, in which κ_p is the phononic contribution to the thermal conductivity and κ_e is the electronic contribution to the thermal conductivity.

We introduce isotropic and adiabatic probe leads on the nanowire, observing little change in nanowire efficiency in the linear response and nonlinear response theory calculations for the parameters we used. However, the difference becomes more profound as the temperature bias increases.

In this thesis causes to submission of one journal paper and our research is going on via temperature bias, and we want to see the temperature bias increases led to a big difference thermopower and thermoelectric efficiency in adiabatic and isotropic cases. Additianally, we want to observe that the thermopower results in the linear and response regime are very near each others at low themperature in terms of adiabatic and isotropic cases. Our continuing research will be prepared to submit to additional one journal paper.

Bibliography

[1] C. B. Vining, "An inconvenient truth about thermoelectrics," *Nature Materials*, vol. 8, pp. 83–85, Feb. 2009.

[2] G. J. Snyder and E. S. Toberer, "Complex thermoelectric materials," *Nature Materials*, vol. 7, pp. 105–114, Feb. 2008.

[3] J.-C. Zheng, "Recent advances on thermoelectric materials," June 2011. J.-C. Zheng, Front. Phys. China, 2008, 3(3): 269-279.

[4] R. Kim, S. Datta, and M. S. Lundstrom, "Influence of dimensionality on thermoelectric device performance," *Journal of Applied Physics*, vol. 105, pp. 034506–034506–6, Feb. 2009.

[5] H. Q. X. Natthapon Nakpathomkun and H. Linke., "Thermoelectric efficiency at maximum power in low-dimensional systems," *Phys. Rev. B*, vol. 82, no. 235428, 2010.

[6] A. I. Hochbaum, R. Chen, R. D. Delgado, W. Liang, E. C. Garnett, M. Najarian, A. Majumdar, and P. Yang, "Enhanced thermoelectric performance of rough silicon nanowires," *Nature*, vol. 451, pp. 163–167, Jan. 2008.

[7] "Silicon nanowires as efficient thermoelectric materials," *Nature*, vol. 451, pp. 168–171, 2008.

[8] C. A. Hewitt, A. Kaiser, M. Craps, R. Czerw, S. Roth, and D. Carroll

[9] G. Pernot, M. Stoffel, I. Savic, F. Pezzoli, P. Chen, G. Savelli, A. Jacquot, J. Schumann, U. Denker, I. MÃ¶nch, C. Deneke, O. G. Schmidt, J. M.

Rampnoux, S. Wang, M. Plissonnier, A. Rastelli, S. Dilhaire, and N. Mingo, "Precise control of thermal conductivity at the nanoscale through individual phonon-scattering barriers," *Nature Materials*, vol. 9, pp. 491–495, June 2010.

[10] H. Sevincli and G. Cuniberti., "Enhanced thermoelectric figure of merit in edge-disordered zigzag graphene nanoribbons," *Phys. Rev. B.*, vol. 81, no. 113401, pp. 1–4, 2010.

[11] G. E. W. Bauer, E. Saitoh, and B. J. van Wees, "Spin caloritronics," *Nature Materials*, vol. 11, pp. 391–399, May 2012.

[12] C. B. Vining, "Materials science: Desperately seeking silicon," *Nature*, vol. 451, pp. 132–133, Jan. 2008.

[13] G. B. Akguc and O. Gülseren, "Thermoelectric efficiency of nanowires with long-range surface disorder," *Phys. Rev. B*, vol. 85, p. 075432, Feb 2012.

[14] G. B. Akguc and J. Gong, "Conductance properties of rough quantum wires with colored surface disorder," *Phys. Rev. B*, vol. 78, p. 115317, Sep 2008.

[15] C. W. J. B. H. van Houten, L. W. Molenkamp and C. T. Foxon, "Enhanced thermoelectric performance of rough silicon nanowires," *Semiconductor Science and Technology*, vol. 7, pp. B215–B221, 1992.

[16] G. B. Akguc and J. Gong, "Wave-scattering formalism for thermal conductance in thin wires with surface disorder," *Phys. Rev. B*, vol. 80, p. 195408, Nov 2009.

[17] D. Roy and A. Dhar, "Electron transport in a one dimensional conductor with inelastic scattering by self-consistent reservoirs," *Phys. Rev. B*, vol. 75, p. 195110, May 2007.

[18] K. Maschke and M. Schreiber, "Unified description of coherent and dissipative electron transport," *Phys. Rev. B*, vol. 44, pp. 3835–3841, Aug 1991.

[19] S. Datta and R. K. Lake, "Voltage probes and inelastic scattering," *Phys. Rev. B*, vol. 44, pp. 6538–6541, Sep 1991.

[20] Y. Ming, Z. X. Wang, Q. Li, and Z. J. Ding, "Nonlinear thermal properties of three-terminal mesoscopic dielectric systems," *Applied Physics Letters*, vol. 91, pp. 143508–143508–3, Oct. 2007.

[21] Y. Ming, Z. X. Wang, Z. J. Ding, and H. M. Li, "Ballistic thermal rectification in asymmetric three-terminal mesoscopic dielectric systems," *New Journal of Physics*, vol. 12, p. 103041, Oct. 2010.

[22] G. Benenti, K. Saito, and G. Casati, "Thermodynamic bounds on efficiency for systems with broken time-reversal symmetry," *Phys. Rev. Lett.*, vol. 106, p. 230602, Jun 2011.

[23] V. Balachandran, G. Benenti, and G. Casati, "Efficiency of three-terminal thermoelectric transport under broken time-reversal symmetry," *Phys. Rev. B*, vol. 87, p. 165419, Apr 2013.

[24] D. Sánchez and L. M. C. Serra, "Thermoelectric transport of mesoscopic conductors coupled to voltage and thermal probes," *Phys. Rev. B*, vol. 84, p. 201307, Nov 2011.

[25] G. B. Akguc and T. H. Seligman, "An efficient method for scattering problems in open billiards: Theory and applications," *Phys. Rev. B*, vol. 74, p. 245317, Dec 2006.

[26] L. E. Reichl, "The transition to chaos: conservative classical systems and quantum manifestations," 2004.

[27] H. Lee and L. E. Reichl, "R-matrix theory with dirichlet boundary conditions for integrable electron waveguides," *Journal of Physics A: Mathematical and Theoretical*, vol. 43, p. 405303, Oct. 2010.

[28] T. E. Humphrey, R. Newbury, R. P. Taylor, and H. Linke, "Reversible quantum brownian heat engines for electrons," *Phys. Rev. Lett.*, vol. 89, p. 116801, Aug 2002.

[29] T. Humphrey and H. Linke, "Reversible thermoelectric nanomaterials," *Physical Review Letters*, vol. 94, Mar. 2005.

[30] W. A. Hofer and A. Garcia-Lekue, "Differential tunneling spectroscopy simulations: imaging surface states," *Phys. Rev. B*, vol. 71, p. 085401, Feb 2005.

[31] K. K. Saha, J. Henk, A. Ernst, and P. Bruno, "Multiple-scattering theoretical approach to scanning tunneling microscopy," *Phys. Rev. B*, vol. 77, p. 085427, Feb 2008.

[32] R. E. Allen, "Green's functions for surface physics," *Phys. Rev. B*, vol. 20, pp. 1454–1472, Aug 1979.

[33] J. N. Schulman and Y.-C. Chang, "Reduced hamiltonian method for solving the tight-binding model of interfaces," *Phys. Rev. B*, vol. 27, pp. 2346–2354, Feb 1983.

[34] N. D. Lang, "Resistance of atomic wires," *Phys. Rev. B*, vol. 52, pp. 5335–5342, Aug 1995.

[35] E. P. Wigner, "Resonance reactions and anomalous scattering," *Phys. Rev.*, vol. 70, pp. 15–33, Jul 1946.

[36] A. M. Lane and R. G. Thomas, "R-matrix theory of nuclear reactions," *Rev. Mod. Phys.*, vol. 30, pp. 257–353, Apr 1958.

[37] K. Varga, "R-matrix calculation of bloch states for scattering and transport problems," *Phys. Rev. B*, vol. 80, p. 085102, Aug 2009.

[38] M. F. O'Dwyer, T. E. Humphrey, and H. Linke, "Concept study for a high-efficiency nanowire based thermoelectric," *Nanotechnology*, vol. 17, p. S338, June 2006.

[39] A. Jeffrey and D. Zwillinger, *Table of Integrals, Series, and Products*. Academic Press, Feb. 2007.

[40] G. B. Akguc and J. Gong, "Spin-dependent electron transport in two-dimensional waveguides of arbitrary geometry," *Phys. Rev. B*, vol. 77, p. 205302, May 2008.

[41] U. Sivan and Y. Imry, "Multichannel landauer formula for thermoelectric transport with application to thermopower near the mobility edge," *Phys. Rev. B*, vol. 33, pp. 551–558, Jan 1986.

[42] P. N. Butcher, "Thermal and electrical transport formalism for electronic microstructures with many terminals," *J. Phys.: Condens. Matter*, vol. 2, pp. 4869–4878, Jun 1990.

[43] S. Datta, "Electronic transport in mesoscopic systems," May 1997.